Deforestation Impacts on Amazon-Andes Hydroclimatic Connectivity

Juan P. Sierra (juan-pablo.sierra-perez@univ-grenoble-alpes.fr)
Université Grenoble 1: Universite Grenoble Alpes https://orcid.org/0000-0001-7001-5943

C. Junquas
Université Grenoble 1: Universite Grenoble Alpes

J. C. Espinoza
Université Grenoble 1: Universite Grenoble Alpes

H. Segura
Université Grenoble 1: Universite Grenoble Alpes

T. Condom
Université Grenoble Alpes: Universite Grenoble Alpes

M. Andrade
Universidad Mayor de San Andres

J. Molina-Carpio
Universidad Mayor de San Andres

L. Ticona
Universidad Mayor de San Andres

V. Mardoñez
Universidad Mayor de San Andres

L. Blacutt
Universidad Mayor de San Andres

J. Polcher
Laboratoire de Météorologie Dynamique: Laboratoire de Meteorologie Dynamique

A. Rabatel
Université Grenoble 1: Universite Grenoble Alpes

J.E. Sicart
Université Grenoble 1: Universite Grenoble Alpes

Research Article

Keywords: Deforestation, high-resolution climate modelling, Amazon basin, Amazon-Andes transition region, energy and water balances.

Posted Date: June 11th, 2021

DOI: https://doi.org/10.21203/rs.3.rs-600041/v1

Deforestation impacts on Amazon-Andes hydroclimatic connectivity

J. P. Sierra[1], C. Junquas[1], J. C. Espinoza[1], H. Segura[1], T. Condom[1], M. Andrade[2], J. Molina-Carpio[2], L. Ticona[2], V. Mardoñez[1,2], L. Blacutt[2,3], J. Polcher[4], A. Rabatel[1], J.E. Sicart[1]

1. Institut des Géosciences de l'Environnement, Université Grenoble Alpes, IRD, CNRS, Grenoble, France.
2. Laboratorio de Física de la Atmósfera, Instituto de Investigaciones Físicas, Universidad Mayor de San Andrés, La Paz, Bolivia.
3. Department of Atmospheric and Oceanic Sciences, University of Maryland, College Park, United States of America.
4. CNRS-IPSL Laboratoire de Météorologie Dynamique (LMD), École Polytechnique, Palaiseau, France.

Main author mail: juan-pablo.sierra-perez@univ-grenoble-alpes.fr

ORCID: https://orcid.org/0000-0001-7001-5943

Abstract

Amazonian deforestation has accelerated during the last decade, threatening an ecosystem where almost one third of the regional rainfall is transpired by the local rainforest. Due to the precipitation recycling, the southwestern Amazon, including the Amazon-Andes transition region, is particularly sensitive to forest loss. This study evaluates the impacts of Amazonian deforestation in the hydro-climatic connectivity between the Amazon and the eastern tropical Andes during the austral summer (December-January-February) in terms of hydrological and energetic balances. Using 10-year high-resolution simulations (2001-2011) with the Weather Research and Forecasting Model, we analyze control and deforestation scenario simulations. Regionally, deforestation leads to a reduction in the surface net radiation, evaporation, moisture convergence and precipitation (~20%) over the entire Amazon basin. In addition, during this season, deforestation increases the atmospheric subsidence over the southern Amazon and weakens the regional Hadley cell. Atmospheric stability increases over the western Amazon and the tropical Andes inhibiting convection in these areas. Consequently, major deforestation impacts are observed over the hydro-climate of the Amazon-Andes transition region. At local scale, nighttime precipitation decreases in Bolivian valleys (~20-30%) due to a strong reduction in the humidity transport from the Amazon plains toward Andes linked to the South American low-level jet. Over these valleys, a weakening of the daytime upslope winds is caused by local deforestation, which reduces the turbulent fluxes at lowlands. These alterations in rainfall and atmospheric circulation could impact the rich Andean ecosystems and its tropical glaciers.

Keywords

Deforestation, high-resolution climate modelling, Amazon basin, Amazon-Andes transition region, energy and water balances.

1. Introduction

The Amazon is the largest tropical rainforest in the world. It exchanges water, energy, and carbon with the

atmosphere and is considered as an essential dynamic component of the climate system (Bonan 2008; Malhi et al. 2008). The Amazon ecosystem has been recognized as one of the major sources of evapotranspiration (Fisher et al. 2011), releasing large amounts of water vapor to the atmosphere and sustaining rainfall not only in the Amazon itself, but also in remote regions of the South American continent (Eltahir and Bras 1994; Van Der Ent et al. 2010; Martinez and Dominguez 2014; Zemp et al. 2014). In addition, the latent heat release linked to moisture recycling over the Amazon basin engines global and regional atmospheric circulation (Gill 1980; Eltahir 1996; Gedney and Valdes 2000). Therefore, understanding the impacts of continued deforestation on the regional and global hydroclimate has become an urgent and extensively explored scientific question.

The Amazonian forest has been intensively cleared since the 1970's (Fearnside 1993; Nepstad et al. 2009). After a slowdown of deforestation rates during the period 2004-2012, the small-scale forest loss rates increased again over the last decade (Kalamandeen et al. 2018; Eiras-Barca et al. 2020). Deforestation, as every effect of human activities on the climate system, disturbs the Earth's radiation budget and can be an important forcing for climate change (Hartmann et al. 2013; Mahowald et al. 2017). Indeed, when the rainforest is replaced by cropland or grassland, the energy balance is disturbed by: (i) a reduction in surface roughness and actual evapotranspiration, decreasing the surface energy loss from turbulent heat removal and latent heat flux (Gash and Nobre 1997; Lee et al. 2011; De Noblet-Ducoudré et al. 2012); (ii) an increase in the incoming solar radiation at the surface linked to less clouds and less evapotranspiration rates (Salati and Vose 1984; Bala et al. 2007); (iii) a reduction in absorbed solar radiation due to an increased surface albedo (Berbet and Costa 2003; von Randow et al. 2004); and finally (iv) less incoming infrared radiation driven by drier air as a result of the reduced evapotranspiration (Eltahir 1996; Claussen et al. 2001). *In-situ* measurements find a decrease in the surface net radiation over cleared areas (Bastable et al. 1993; von Randow et al. 2004). Although at the annual time scales an air temperature warming of the layer close to the surface follows the forest clearance (Gash and Nobre 1997), the reduction in the net surface radiation generates a cooling of the upper atmosphere and a subsidence that weakens the regional circulation (Eltahir 1996). In this sense, perturbations that initially occurs at the surface and within the lower part of the atmosphere modify the vertical transport of heat and moisture, altering convection and subsidence over extended regions and affecting large-scale features such as the Hadley and Walker cells (Zhang et al. 1996; Snyder 2010; Badger and Dirmeyer 2015).

Atmospheric circulation and Amazonian rainforest compound a coupled bio-geophysical balanced system. Perturbations in the vegetation state through deforestation can drive very different changes in atmospheric circulation depending on its spatial scale. Observations and theoretical works show small-scale deforestation (<10km) triggering thermally driven land breeze resulting from differences in sensible heat fluxes between pastured and forested areas (Pielke, R. A. 1984; Atkinson 1989; Wang et al. 1996; Souza et al. 2000; Pielke 2001; D'Almeida et al. 2007; Lawrence and Vandecar 2015). However, thermally driven circulations seem to be scale-dependent and can weaken as deforestation areas increase (Avissar and Schmidt 1998; Patton et al. 2005). At spatial scales larger than 100 km, land surface heterogeneities cannot produce enough surface gradient to sustain thermal circulation (Dalu and Pielke 1993). In fact, a recent study in Rondonia-Brazil demonstrates how when cleared areas grow, a shift occurs from a thermally convective regime towards a dynamically driven state where the roughness length reduction dominates and favors (inhibits) convection over areas in the downwind (upwind)

direction of the deforested zone (Khanna et al. 2017). Since deforestation impacts in hydrological and atmospheric processes are complex and scale dependent, regional and global climate models stand out as useful tools to better understand the response of the climate system to land-use perturbations.

Numerical climate models have been extensively used for analyzing the impacts of deforestation over regional and global climate (Nobre et al. 2016 and references therein). Mesoscale models are able to represent the observed changes in circulation and clouds that follow small-scale deforestation (Chen and Avissar 1994; Wang et al. 2000; Saad et al. 2010). Furthermore, the thermal-to-dynamical shift regime caused by the rainforest loss reported over south-western Brazil is also reproduced by these models (Khanna et al. 2017). Under different deforestation scenarios, models project more frequent dry events and a lengthening of the Amazonian dry season (Nobre et al. 1991; Bagley et al. 2014; Alves et al. 2017; Ruiz-Vásquez et al. 2020; Costa and Pires 2010). Although recent observational studies report similar changes in Amazonian dry season hydrology since 1979, the attribution of these alterations to deforestation is not straightforward and evidence suggest an additional influence of the tropical north Atlantic Ocean warming (Fu and Li 2004; Yoon and Zeng 2010; Butt et al. 2011; Marengo et al. 2011; Fu et al. 2013; Debortoli et al. 2017; Espinoza et al. 2019a; Leite-Filho et al. 2020). It is important to remark that, taking into account the dependency of climate response to the size of deforestation, the current spatial scale of Amazonian cleared area is not enough for predictions of extreme deforestation scenarios to be manifested or detected (D'Almeida et al. 2007; Nobre et al. 2016). On the other hand, under extensive deforestation scenarios climate models predict a reduction in precipitation recycling and rainfall in places downstream of the cleared areas caused by the shut off of forest transpiration (D'Almeida et al. 2007; Moore et al. 2007; Correia et al. 2008; Swann et al. 2015). At the same time, empirical estimates have found that south-western Amazon is particularly dependent on evapotranspiration from other parts of the basin (Zemp et al. 2017a; Staal et al. 2018). Hence, several simplified and regional climate models present a decreasing in rainfall and moisture transport over this particular area (Sun and Barros 2015a; Boers et al. 2017; Zemp et al. 2017b; Ruiz-Vásquez et al. 2020). However, an opposite effect of intensified moisture transport towards south-western Amazon and south-eastern South America has been suggested by some modelling studies as the result of deforestation induced decreasing in surface roughness (Lean and Rowntree 1997; Eiras-Barca et al. 2020). These different responses to similar deforestation scenarios suggest the need to further assess the impacts of Amazon forest clearance over the regional climate.

In the Amazon-Andes transition region lies the rainiest and biologically richest area of the entire Amazon basin (Myers et al. 2000; Killeen et al. 2007; Hoorn et al. 2010; Espinoza et al. 2015). This region encompasses complex Andean topography, ranging between almost sea level in the Amazon lowlands to more than 6000 m a.s.l. over the Andean summits. This causes a strong orographic effect that interacts with regional atmospheric circulation to produce an exceptional spatial rainfall contrast (Chavez and Takahashi 2017; Junquas et al. 2018). There, high precipitation rates lead to large values of runoff per unit area (Moquet et al. 2011), providing most of the sediment load to Amazon rivers (Vauchel et al. 2017; Armijos et al. 2020). Consequently, extreme hydrological events over this region can impact the whole basin downstream (Espinoza et al. 2014). Particularly, the Amazon-Andes transition region exhibits the largest precipitation recycling (portion of the precipitated water previously transpired by the Amazonian rainforest) of the Amazon catchment (Eltahir and Bras 1994; Dirmeyer and Brubaker 2007; Van Der Ent et al. 2010; Staal et al. 2018). Therefore, this region can potentially be highly sensitive to Amazon

deforestation effects. Nevertheless, the surface-atmosphere coupling over this area has been poorly studied and most of the referent work has been focused over Brazilian Amazon or was based on coarse horizontal resolution modelling experiments insufficient to capture the required details of the topographical influence on local convection.

This study aims to better understand the deforestation effects on moisture transport and rainfall over the Amazon-Andes transition region during the wet season (December-January-February, DJF). During this season nearly 50% of total annual precipitation falls over the region (Espinoza et al. 2009). Since Amazonian groundwater recharge during wet periods can sustain forest transpiration rates during dry months (Miguez-Macho and Fan 2012), DJF alterations in rainfall patterns may have a profound impact in the watershed hydrology. The strong summer convection in the region is controlled by atmospheric processes that are part of the development of the South American Monsoon System (SAMS; Vera et al. 2006; see section 3.1 for details) and which may be sensitive to impacts on surface energy/water fluxes induced by land use change (Li and Fu 2004).

Taking into account the potential sensitivity of the Amazon-Andes transition region to deforestation and the need for high-resolution studies, the present work analyzes the deforestation land-use change impacts on regional energy and water budgets, as well as rainfall alterations at a local scale through the use of high-resolution simulations (up to 1km horizontal grid size) with the regional climate model Weather Research and Forecasting Model (WRF). Model hourly outputs are compared with observational data from rain-gauges and satellites in order to elucidate the possible changes caused by Amazonian deforestation in the diurnal and nocturnal precipitation inside a typical Andean valley during 2001-2011 austral summer. We describe the configuration of the model, the deforestation experiment and reference data used in Sect. 2. In Sect. 3, we validate the model skill to reproduce the precipitation, general circulation and moisture transport at regional scale, as well as its ability to properly represent the deforestation signal in comparison with observations from the LBA project. The impacts of deforestation on moisture transport and rainfall at regional, meso and local scales are analyzed in Sect. 4. Finally, Sect. 5 summarizes and discusses the main results.

2. Data and Methods

2.1 Model Description

This study uses the regional climate model WRF version 4.1 (Skamarock et al. 2019). The model WRF was used in previous works to study the climatology of tropical South America and the Amazon basin (Bagley et al. 2014; Sun and Barros 2015a, b; Mourre et al 2016; Junquas et al 2018; Heredia et al. 2018; ; Spera et al. 2018; Trachte 2018; Yang and Dominguez 2019; Eiras-Barca et al. 2020; Saavedra et al. 2020). WRF is a nonhydrostatic model with terrain-following vertical levels (we use 49 vertical levels with higher level density near the surface). We employ three one-way nested modelling domains as shown in Figure 1c. Table 1 summarizes the information of spatial and temporal resolution for each of the three domains used in this work. The first domain encompasses tropical South America and has a horizontal resolution of 15 km x 15 km with a time step of 90 seconds. The second and third domains have a spatial resolutions of 5 km x 5 km and 1 km x 1 km, respectively and cover the south-western part of the basin. Time steps for these two domains are 30 seconds and 6 seconds, respectively. Domain 3 comprises the instrumented Andean valleys of Zongo and Huarinilla used for model validation (Fig.

1d). In order to analyze the diurnal and nocturnal atmospheric conditions we use an output time resolution of 3 hours for domains 1 and 2, and 1 hour for the finest domain.

Lateral boundary conditions from ERA5 reanalysis (Hersbach et al. 2020) are used. This reanalysis presents an enhanced horizontal resolution of 0.28° x 0.28° (31 km) with data available every 6 hours (https://www.ecmwf.int/en/forecasts/datasets/reanalysis-datasets/era5). Significant improvements in the representation of several model processes in this reanalysis are reflected in a better fit in winds, temperature and humidity in the troposphere compared against radiosonde data (Hersbach et al. 2020).

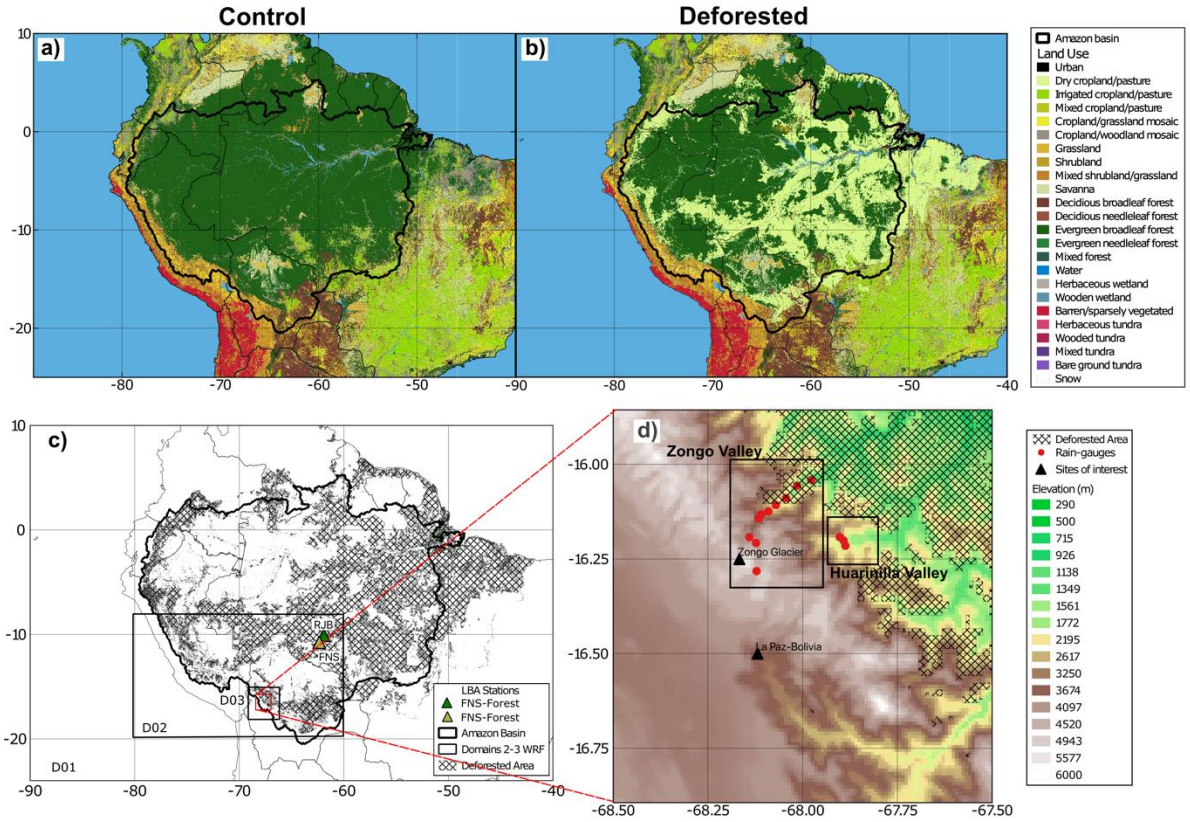

Fig 1 Land-use category distributions for: a) Control and b) Deforested scenarios. c) Deforested area and locations of selected flux towers from the Large-Scale Biosphere-Atmosphere Experiment in the Amazon. Black boxes show WRF domains. Delineated area represents the boundary of the Amazon River basin (black). d) D03 subregion and locations of rain-gauges stations over two Andean mountain valleys

Preliminary tests for different model configurations (not shown) allow selecting the parameterizations shown in Table 2. Summarizing, we use the Yonsei University scheme for representation of the boundary layer (Hong et al. 2006) with the wind topographic correction activated (Jiménez and Dudhia 2012). This wind correction takes into account the momentum sink term generated by the unresolved terrain at sub-grid scale in the model. It has shown improvements in the simulated wind field over complex terrains (Jiménez and Dudhia 2012) and has already been tested in the tropical Andes (Junquas et al. 2018). Lin's microphysics scheme is implemented (Lin et al. 1983) for phase change and precipitation. We also use Grell 3D parametrization for sub-grid scale convection over domains 1 and 2 (Grell and Dévényi 2002). Previous studies demonstrate convection parametrizations as one

of the major uncertainties in the representation of rainfall diurnal cycle (Brockhaus et al. 2008; Hohenegger et al. 2008). Taking this into account and considering that a spatial resolution higher than 4 km is considered enough for non-hydrostatic models to explicitly solve convection (Weisman et al. 1997; Ramos da Silva and Avissar 2006), we deactivate the cumulus parameterization over the finest domain.

In order to obtain a climatological state of the south-western Amazon wet season, our simulations cover 10 years of austral summers for the time period 2001-2011. Each simulation starts on November 1st and the first month is removed as a spin-up for the output analysis.

2.2 Description of the experiments

For each austral summer in the period 2001-2011, we conduct two simulations with WRF sharing the same atmospheric lateral boundary conditions, but with different land-cover states. The control simulation ("Control" or "Con") corresponds to vegetation conditions for the year 2000 using the land cover map developed for South America by Eva et al. (2004) (Fig. 1a). This dataset was implemented in WRF by Saavedra et al. (2020) and exhibits a spatial resolution of 1 km x 1km. For the deforested simulation ("Deforested" or "Def"), we use the deforested scenario 2050 business-as-usual from Soares-Filho et al. (2006; Fig. 1b). This scenario reaches 45% of forest lost and assumes the continuation of the 1997-2002 registered deforestation rates, no definition of new protected areas in the basin and the building of all planned highways (Soares-Filho et al. 2006). This scenario does not include the forest impoverishment through logging and fires. The implemented deforestation polygon is shown in Fig. 1c. Amazon deforestation involves the replacement of native forest by mixed crops (mainly soybean and corn), as well as pasture for cattle feeding. For this reason, within the deforested polygon natural forest grid points are replaced by cropland/grassland mosaics.

Table 1. Characteristics of the domains used in WRF simulations.

	WRF-D01	**WRF-D02**	**WRF-D03**
Horizontal resolution (km)	15	5	1
Domain	Tropical South America	South-western Amazon	Bolivian Andean valleys
Domain center coordinates	7° 30' 00" S, 65° 00' 00" W	13° 56' 12" S, 70° 4' 49" W	16° 35' 49" S, 67° 38' 56" W
Configuration	Regional simulation	One-way nesting	One-way nesting
Forcing	ERA5	WRF-D01	WRF-D02
Vertical resolution	49 hybrid vertical levels	49 hybrid vertical levels	49 hybrid vertical levels
Run time step (s)	90	30	6
Output time resolution (h)	3	1	1

Table 2. Physical parameterizations used in WRF simulations.

	Parameterizations	**References**

Radiation	Longwave: rapid radiative transfer model (RRTM)	(Mlawer et al. 1997)
	Shortwave: Dudhia scheme	(Dudhia 1989)
Cumulus	Grell 3D	(Grell and Dévényi 2002)
Planetary boundary layer	Yonsei University scheme	(Hong et al. 2006)
Land surface	Noah land surface model	(Chen and Dudhia 2001)
Cloud microphysics	Lin scheme	(Lin et al. 1983)
Surface layer	MM5 similarity	(Paulson 1970)

2.3 Data

In order to validate the model's ability to represent the rainfall spatial distribution in the region, we use the product Tropical Rainfall Measuring Mission 3B42 (TRMM; https://disc.gsfc.nasa.gov). This dataset, available from 1998, presents a 0.25° x 0.25° resolution and includes precipitation rates every 3 hours (Huffman et al. 2007). However, previous studies have identified a strong rainfall underestimation by TRMM in the Amazon-Andes region (Espinoza et al. 2015; Zubieta et al. 2015; Chavez and Takahashi 2017). For this reason, we complement the model validation with daily information of 10 rain-gauge stations (Fig. 1d) from the Bolivian Electric Power Company (COBEE) and managed in collaboration with the Institute of Research for the Development (IRD) - France. Additionally, three stations with hourly data were used from Schwabe et al. (2011). Table 3 presents the general information of each rain-gauge station. The quality assessment of these rainfall stations was carried out by previous works (Molina-Carpio et al. 2019 and Laura Ticona, personal communication). The use of *in-situ* information also allows characterizing the model skill to capture the precipitation variability at small spatial scale in an Andean valley where local processes are important (Egger et al. 2005; Trachte et al. 2010; Junquas et al. 2018). Additionally, the representation of the regional atmospheric circulation and moisture transport are validated by a direct comparison between WRF outputs and ERA5 data.

To test whether WRF responds realistically to the changes induced by land-use alterations, we use observations of energy surface fluxes, air temperature, precipitation and wind speed from the LBA project (Saleska et al. 2013). This dataset is available at the website https://daac.ornl.gov/LBA/guides/CD32_Brazil_Flux_Network.html. The Large-Scale Biosphere-Atmosphere (LBA) project was a large scientific effort carried between 1996 and 2006 for assessing the influence of tropical forest conversion in carbon storage, nutrient dynamics and trace gas fluxes in the Amazon. Since the region of interest of this study is the Amazon-Andes transition region, we only use the closest stations from the LBA project that fits inside our second modelling domain (Fig. 1c). Because of their geographical location, these stations experience annual cycles of precipitation and temperature similar to the south-western Amazon variability. The first station, *Fazenda Nossa Senhora de Aparecida* (yellow triangle labeled as "FNS" in Fig.1c), is a cattle ranch located at the center of a deforested area of about 50 km in radius cleared in 1977 for crop cultivation. The tower flux stands at 306 m a.s.l., 10.75°S, 62.35°W and presents daily data for the period 1999-2002. The second station corresponds to *Rondonia Jaru Biological Reserve* and is located at 191 m a.s.l., 10.08°S, 61.93°W (green triangle labeled as "RJB" in Fig.1c). This is a natural reserve of the Brazilian Environmental Protection Agency covered by tropical dry forest with a mean tree height of 33 m that was established in the 1960s and expanded in 2006. The proximity of these stations (around 87 km) allows to test

the impacts of land use change on surface fluxes and the atmospheric bottom conditions. For validation we only use data for DJF 2001-2002 when WRF simulations and LBA data availability periods overlap in time.

Table 3. Name, geographic location, elevation, temporal range and annual rainfall of rain-gauge stations.

Name of station	**Location (latitude, longitude)**	**Elevation (m a.s.l.)**	**Temporal period (years)**	**Annual (DJF) rainfall in mm/year(mm/month)**
Plataforma	16.28° S, 68.12° W	4719	1971-2018	691 (138)
Tiquimani	16.20° S, 68.12° W	3997	1971-2018	918 (196)
Botijlaca	16.19° S, 68.14° W	3557	1971-2018	983 (178)
Cuticucho	16.14° S, 68.11° W	2790	1971-2018	2053 (341)
Santa Rosa	16.13° S, 68.10° W	2659	1971-2018	1748 (317)
Sainani	16.12° S, 68.09° W	2224	1971-2018	1975 (358)
Chururaqui	16.10° S, 68.07° W	1867	1971-2018	2086 (334)
Harca	16.08° S, 68.04° W	1546	1971-2018	2061 (358)
Cahua	16.05° S, 68.01° W	1271	1981-2018	2595 (405)
Huaji	16.04° S, 67.97° W	1043	1999-2018	2676 (454)
Hornuni 1800	16.19° S, 67.90° W	1800	2001-2002	2310 (311)
Hornuni 2600	16.20° S, 67.89° W	2600	2001-2002	3970 (489)
Hornuni 3010	16.21° S, 67.88° W	3010	2001-2002	5150 (651)

2.4 Calculation of energy/water balances and atmospheric stability

The energy budget at the surface is described by (Duveiller et al. 2018):

$$N_R = (S_{in} - S_{out}) + (L_{in} - L_{out}) = Sens_H + Lat_H + Gr_H \quad (1)$$

Here, N_R corresponds to net radiation and is the summation of contributions from shortwave and longwave components: S_{in} is the incident shortwave or solar radiation, S_{out} is the reflected solar radiation, L_{in} is the incoming longwave component and L_{out} is the emitted longwave radiation flux. The net turbulent heat flux is later distributed in sensible heat flux ($Sens_H$), latent heat flux associated with evaporation from the surface (Lat_H) and molecular conduction flux from the ground (Gr_H). All the terms in Eq. (1) are in W/m^2. Land use change disturbances in the energy budget are assessed computing the differences in DJF climatological means for each term of Eq. (1) between Deforested and Control scenarios.

The atmospheric water budget establishes how precipitation, evapotranspiration and net moisture transport entering/leaving an atmospheric column controls the temporal changes in the vertically integrated water content (Peixoto and Oort 1992). At seasonal timescales the temporal changes in atmospheric moisture are negligible and precipitation, evapotranspiration and column moisture convergence nearly balances each other (Brubaker et al. 1993; Li et al. 2013). Hence, the climatological changes induced by deforestation in the water balance can be expressed as follows:

$$\Delta\overline{P}_{Def-Con} = \Delta\overline{E}_{Def-Con} - \frac{1}{g}\Delta\overline{\nabla \cdot \int_{1000_{hPa}}^{200_{hPa}} q\,\vec{V}_H dp}_{Def-Con} \qquad (2)$$

In Eq. (2), P is precipitation, E is evapotranspiration and $\nabla \cdot \int_{1000_{hPa}}^{200_{hPa}} q\,\vec{V}_H dp$ is the divergence field of vertically integrated moisture flux from 1000 hPa to 200 hPa. The bars denote climatological DJF means.

Finally, we evaluate the deforestation impacts on the atmospheric stability in tropical South America. Over the Amazon, the moistening of mid-tropospheric levels is associated with the development of deep convection in the region, which is related to the decreasing of atmospheric stability between middle and upper levels of the troposphere (Scala et al. 1990; Zhuang et al. 2017). For this reason, recent works use the difference of equivalent potential temperature (θ_e) between middle (500 hPa) and upper (200 hPa) troposphere ($\theta_{e_{200-500}}$) as an atmospheric stability index (Segura et al. 2020). The equation of equivalent potential temperature can be written following Stull and Ahrens (2000):

$$\theta_e = \theta + \left(\frac{L_V \theta}{C_P T}\right) r \qquad (3)$$

where, θ corresponds to potential temperature, L_V is the latent heat of vaporization, C_P is the specific heat for air at constant pressure, T corresponds to the air absolute temperature and r is the air mixing ratio. The first term of this equation is related with dry adiabatic processes while the second one includes the effect of moisture in the net energy of an air parcel. Thus, the changes in the difference between mid and upper tropospheric equivalent potential temperature ($\theta_{e_{200-500}}$) allows separating the individual effects of dry and wet processes in the regional atmospheric stability. Again, climatological mean differences in each term of Eq. (3) between Deforested and Control scenarios allow evaluating the impact of deforestation in the regional atmospheric stability.

3. Model validation

3.1 Regional scale

The development of the SAMS establishes a northerly cross-equatorial flow (Wang and Fu 2002) and enhances convection over central Amazon (Vera et al. 2006; Figs. 2a, c). A cloudiness/rainfall band known as the South Atlantic Convergence Zone (SACZ) extends from southern Amazonia towards south-eastern Brazil and accompanies the mature phase of the SAMS (Kodama 1992; Figueroa et al. 1995; Zhou and Lau 1998; Fig. 2a). The diabatic heating released by the convective activity generates a large anticyclonic circulation at the upper troposphere centered around 15°S - 65°W known as the Bolivian High (Lenters and Cook 1997; Fig. 2e). Latent heat release over central Amazon also promotes a low-level continental-scale gyre that transports water vapor from the Atlantic Ocean inland towards Amazon and La Plata basins (Rodwell and Hoskins 2001; Vera et al. 2006; Fig. 2c). Over the eastern flank of the Andes, this circulation reaches its maximum wind velocities forming the South American Low-Level Jet (SALLJ). Over its trajectory, the transport of moisture through the SALLJ encounters the topographical barrier of the Andes triggering forced convection in very localized places or rainy hotspots mainly in the Bolivian and Peruvian piedmonts (Espinoza et al. 2009; Espinoza et al. 2015; Chavez and Takahashi 2017; Fig. 2a).

In general terms, the model is able to reproduce the main precipitation features during the austral summer (Fig. 2b). WRF-D01 represents the strong precipitation over central Amazon but with its maximum shifted eastward. The characteristic northwest-southeast rainfall band of the SACZ is present in WRF simulation. However, the model shows a considerable negative bias over the northern Peruvian lowlands (until -50% of dry bias when compared to TRMM; red contours in Fig. 2b). Rainfall Peruvian and Bolivian hotspots are also part of the model climatology. Nevertheless, WRF underestimates the former and overestimates the latter. The Atlantic ITCZ is strongly overestimated by WRF (up to +200% with respect to TRMM; red contours in Fig. 2b). This wet bias is related to a too strong vertically integrated moisture convergence in the model output (Fig. 2d). Finally, upper and lower atmospheric circulations are realistically represented by WRF (Fig. 2d, f). As in ERA5 outputs, WRF easterly low-level winds carry moisture from the Atlantic Ocean toward the continent (Fig. 2d). The moisture flow moves parallel to the Andes cordillera mechanically deviated exporting humidity toward southern latitudes both for ERA5 and WRF. At the altitude of 200 hPa, the model develops the anticyclonic circulation of the Bolivian High (Fig. 2f).

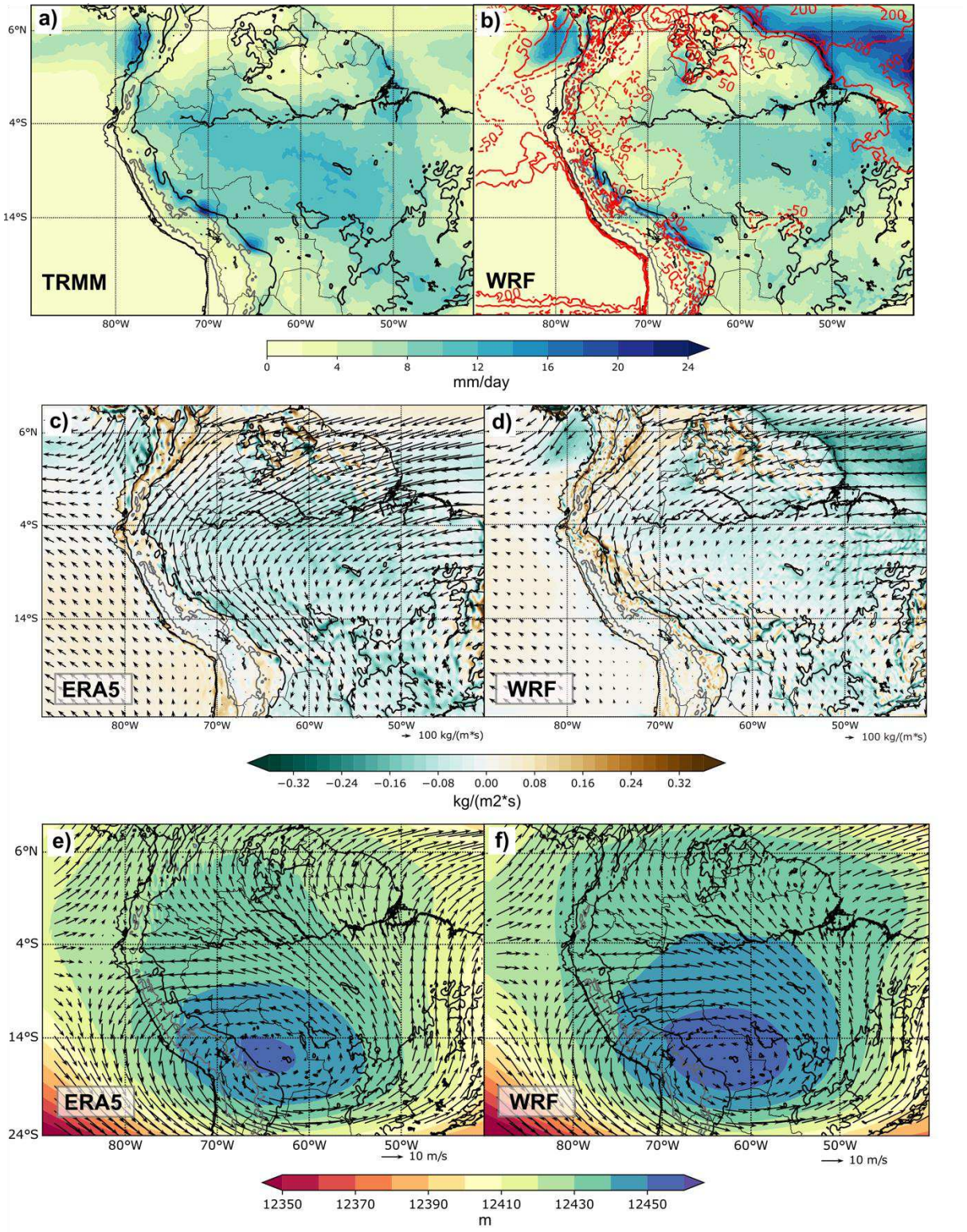

Fig 2 DJF climatological means over the period 2001-2011 for: a) and b) precipitation from TRMM-3B42 (a) and WRF-Control (b) in mm/day. Red lines in b represent rainfall differences respect to TRMM in percentage. c) and d) vertically integrated moisture flux (vectors, kg/m*s) and its divergence (shaded, kg/m^2*s) from ERA5 (c) and WRF-Control (d). e) and f) horizontal winds at 200 hPa (vectors, m/s) and geopotential height (shaded, m) from ERA5 (e) and WRF-Control (f). Orography elevation is shown at 500 and 3500 m a.s.l. as black and grey contours, respectively

3.2 Local scale

In order to validate if WRF reproduces the observed land use change impacts in surface fluxes and atmospheric variables at a local scale, we compare the selected LBA stations (section 2.3) against the WRF-D02 Control simulation for DJF 2001-2002. We take the paired pasture/rainforest sites from the LBA project and compute the observed changes in surface variables in percentage respect to the forest values. Then, similarly, we take the coordinates of the LBA pasture and rainforest stations and extract information of atmospheric variables from model outputs in order to compute the percentage changes. For WRF outputs, we average variables of interest around each location inside a surrounding area of 15 km x 15 km (one grid-point-radius) but selecting only the grids corresponding to cropland/grassland or forest respectively and ignoring grid cells with a different land use category. Between a 15km radius and a 50km radius, no significant changes are found in the WRF deforestation response (not shown).

Figure 3 shows the simulated and observed (orange and blue bars, respectively) mean differences of surface variables due to deforestation. Significant differences are highlighted in red contour according to a t-test ($p<0.05$). In general terms, WRF is able to properly represent the nature of most of the alterations in surface fluxes and atmospheric variables induced by the land use change. Land cover change is related to reduced precipitation by around -44% and -30% in observations and WRF, respectively. However, since precipitation is also related with non-local processes, it is difficult to establish a deforestation-rainfall causality relation. Consistently, significant reductions in surface specific humidity are observed but weakly simulated (around -11% and -1% in observations and WRF, respectively). Accordingly, there is a significant decrease in latent heat flux for observations (-37%) with a weaker response by WRF (-14%). This implies that WRF underestimates the evapotranspiration response induced by deforestation. There is a significant increase in sensible heat flux and surface air temperature in LBA stations (+68% and +1%, respectively). WRF strongly underestimates the sensible heat increase and even slightly invert the temperature response to land use change (+1.49% and -0.02% respectively). The effects of the increased sensible heat and temperature (only sensible heat in WRF) act to give an increase in the outgoing longwave radiation flux in LBA stations of +1.6% (+0.7% in WRF). Since pastures and croplands are brighter than forest (Oguntoyinbo 1970; Bonan 2008), an increase in the albedo rises the outgoing or reflected shortwave radiation in +86% for observations (Loarie et al. 2011). The albedo effect is overestimated by WRF, which presents an outgoing shortwave radiation pasture/forest difference of +104%. This overestimated energy loss can be related with the model underestimation of sensible heat flux increase. More incoming shortwave radiation reaches the surface in model and observations (+4% and +7% respectively). This difference in WRF simulation is a consequence of cloud reduction over deforested areas (not shown). There is a disagreement between the modelled and observed changes in the incoming longwave radiation. While WRF exhibits a decrease in this variable (-1.64%), observations report an increase of about +1.38%. This difference is possibly explained by biases in the model representation of clouds or because of the drier WRF mid-upper troposphere (not shown). At the end, driven by the incremented energy losses through longwave radiation fluxes and shortwave radiation reflection, there is a reduction in net radiation for WRF (-15%) and LBA stations (-8%). Finally, the enhanced surface wind speed at 2 m is a direct consequence of the deforestation induced roughness-length reduction in both model (+53%) and observations (+95%).

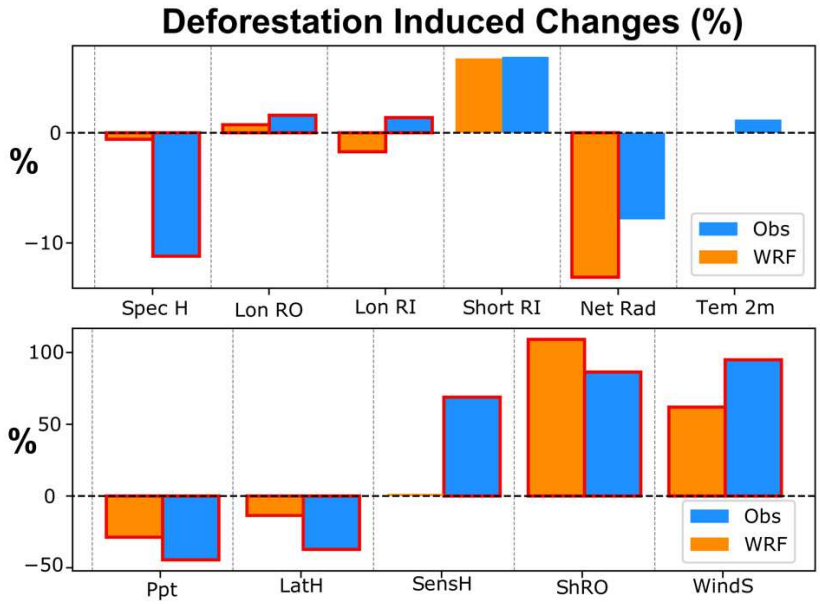

Fig 3 Deforestation induced changes in surface atmospheric variables over LBA stations (blue bars) and WRF-D02 (orange bars) for DJF in the period 2001-2002. Significant differences are delineated in red (t-test, $p<0.05$). Abbreviations are as follows: Spec H - specific humidity at 2 m, Lon RO – longwave outgoing radiation, Lon RI – longwave incoming radiation, Short RO – shortwave outgoing radiation, Short RI – shortwave incoming radiation, Net-Rad – net radiation, Tem2 2m – air temperature at 2 m, LatH – latent heat flux, SensH – sensible heat flux, Ppt – precipitation, WindS – wind speed at 10 m

4. Results and discussion

This section is composed of two subsections, in the first part we evaluate the effects of deforestation in the energy and water balances, as well as the atmospheric stability at regional-scale (90°-60° W, 24° S-9° N). The second subsection is focused on the alterations in the hydro climatology at meso and local scales, especially over the Amazon-Andes transition region and Andean valleys of Bolivia.

4.1 Regional changes in energy and water balances

Climatological alterations in the surface energy balance (Eq. (1)) induced by deforestation are shown in Figure 4, in which significant differences are highlighted with black slashes. The last term in Eq. 1 corresponding to soil heat flux is omitted because it exhibits much smaller magnitudes with respect to the other terms ($\pm$1W/m^2). Indeed, in situ measurements report low soil heat fluxes below tropical forest (Shuttleworth et al. 1984), but important values for crops (Oliver et al. 1987; Gash and Shuttleworth 1991).

Important changes in the incoming solar radiation are induced by the forest loss in the region (Fig. 4a). In general, more (less) incident solar radiation reaches the ground over places where reduction (rise) in precipitation and moisture convergence are located (see Fig. 5) such as in the central and south-western Amazon (north of South America and eastern Brazil). Hence, disturbances in incident solar radiation are closely linked with changes in clouds in WRF simulations as confirmed by analyzing top of the atmosphere (TOA) outgoing longwave flux and cloud water content (not shown). However, major changes in the energy balance occur in the outgoing shortwave

radiation (Fig. 4b). A significant increase in about +20 W/m^2 occurs only over deforested areas which reflects the very local response induced by the higher cropland/grassland albedo. With a minor response, reductions in the longwave incoming radiation occur over most of the Amazonian watershed (Fig. 4c) as a result of a drier atmosphere and lower cloud cover in the deforested scenario (not shown). On the other hand, there is a meridional dipole in longwave outgoing radiation changes (Fig. 4d). Important disturbances in this variable take place mainly over deforested areas which implies the influence of very local processes. North of the Amazon river (<5°S) at the East of the basin, upward longwave radiation increases as a consequence of an increase in surface emissivity over this area (not shown). However, in the southern part of the basin, less outgoing longwave radiation is related to reductions in sensible heat flux and air surface temperature. Sensible heat disturbances are linked to surface air temperature changes (not shown). Thereby, reductions (increments) in this turbulent flux are located over deforested areas (Fig. 4e) and are related with decreasing (increasing) surface temperature (not shown). Similarly, latent heat flux decreases over regions with evapotranspiration reductions (Figs. 4b,5b). In the end, the enhanced energy loss through reflected shortwave radiation as well as the reduced incoming longwave radiation flux decrease the surface net radiation over the deforested and surrounding areas (Fig. 4g). This reduction in net radiation is very important for driving alterations in the regional moisture convergence as pointed out by Zeng and Neeling (1999). It is important to remark that the overestimation of the albedo effect and the weaker model responses in sensible heat and longwave outgoing radiation fluxes, as well as roughness length and surface wind velocity (see section 3.2) constrain our conclusions in the following sections.

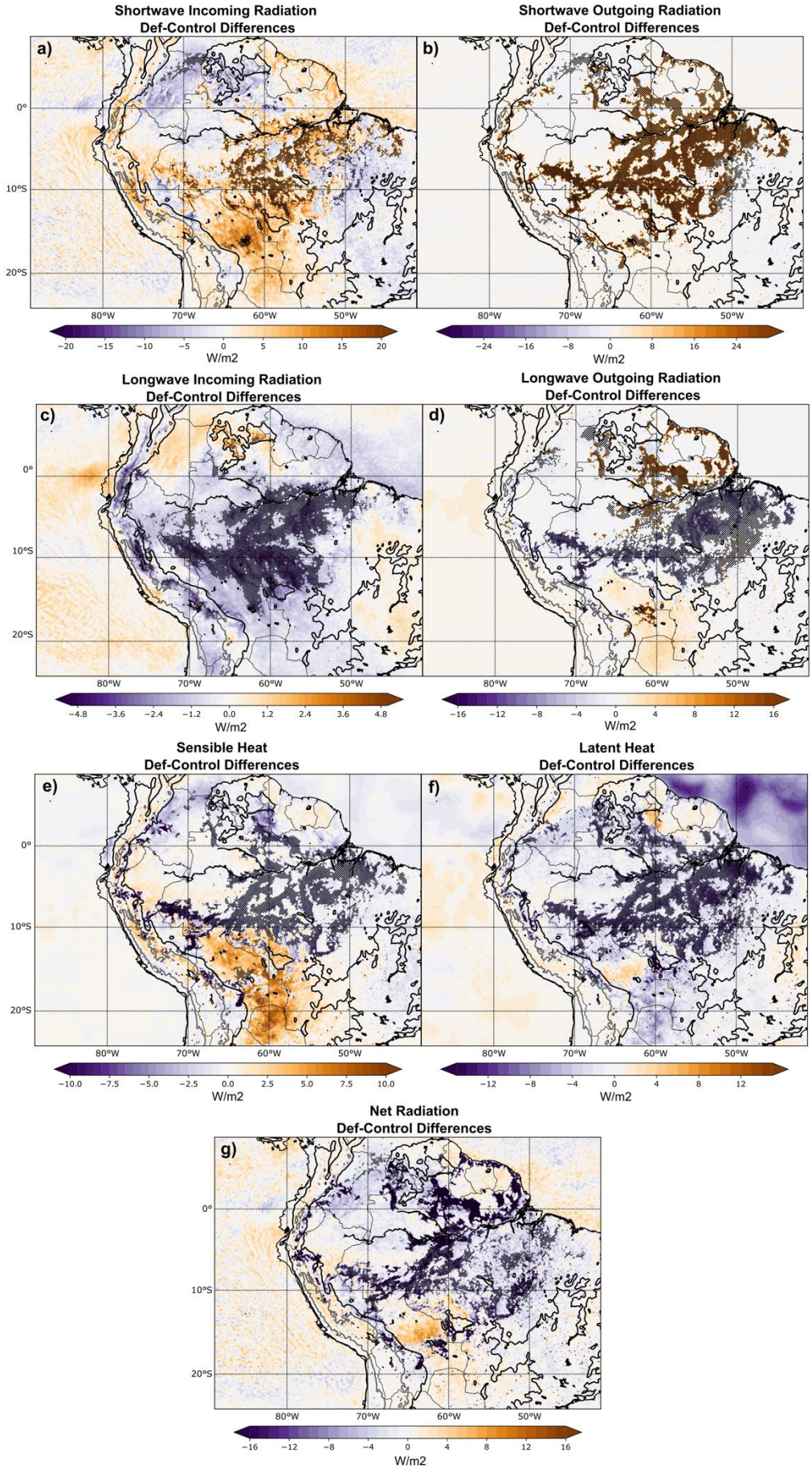
Shortwave Incoming Radiation
Def-Control Differences
a)
Shortwave Outgoing Radiation
Def-Control Differences
b)
Longwave Incoming Radiation
Def-Control Differences
c)
Longwave Outgoing Radiation
Def-Control Differences
d)
Sensible Heat
Def-Control Differences
e)
Latent Heat
Def-Control Differences
f)
Net Radiation
Def-Control Differences
g)
0°
10°S
20°S
80°W
70°W
60°W
50°W
W/m2

414

Fig 4 DJF seasonal climatological differences Deforested minus Control during 2001-2011 in surface energy balance variables: a) Shortwave incoming radiation ($\Delta\overline{S_{in}}_{Def-Con}$). b) Shortwave outgoing radiation ($\Delta\overline{S_{out}}_{Def-Con}$). c) Longwave incoming radiation ($\Delta\overline{L_{in}}_{Def-Con}$). d) Longwave outgoing radiation ($\Delta\overline{L_{out}}_{Def-Con}$). e) Sensible heat flux ($\Delta\overline{Sens_H}_{Def-Con}$). f) Latent heat flux ($\Delta\overline{Lat_H}_{Def-Con}$). g) Net radiation ($\Delta\overline{NR}_{Def-Con}$). All figures are in W/m^2. Significant changes (t-test, $p<0.05$) are marked with black slashes. Orography elevation is shown at 500 and 3500 m a.s.l. as black and grey contours, respectively

Figure 5 shows simulated changes in the water balance following Eq. (2). Significant reductions in the seasonal rainfall are found over central and south-western Amazon closely matching the deforestation area (Fig. 5a). To some extent, these precipitation changes are related to the local impact of the decreased evapotranspiration, especially over the center of Brazilian Amazon (Fig. 5b). However, the drier conditions over Bolivian Amazon are closely linked with changes in the regional atmospheric circulation, where increased moisture divergence is a response to deforestation (Fig. 5c). The decrease in moisture convergence and rainfall over most of the Amazon also implies a reduction in the vertical velocity (Fig. 5d), a rise in the atmospheric pressure at lower levels (not shown), and a weakening of the regional Hadley cell (Fig. 5e). These changes are in agreement with the theoretical frameworks laid out by Gill (1980) and Eltahir (1996), and with modelling studies (Zhang et al. 1996; Sun and Barros 2015a; Badger and Dirmeyer 2016). Opposite to the forcing in Gill (1980), Amazon deforestation induces a lack of diabatic heating as a result of a drier atmosphere and less convection in the region (Eltahir 1996; Badger and Dirmeyer 2016). This feature is observed in Figure 5e as a drier troposphere below 650 hPa over 10°S-18°S and as an enhanced subsidence over the same latitudinal band. These changes are also associated with slightly stronger westerlies at the upper troposphere and a small weakening of the Bolivian High (not shown). Similar changes in the regional circulation and in the regional Hadley cell have been reported by previous modelling and theoretical studies (Zhang et al. 1996; Eltahir 1996; Zeng and Neelin 1999; Badger and Dirmeyer 2016). In the linear model developed by Eltahir (1996), the tropical subsidence is a consequence of a reduction in the boundary layer entropy that follows large-scale deforestation. On the other hand, according to Zeng and Neelin (1999) and in agreement with Figure 4, reductions in rainfall and moisture convergence over the Amazon basin induced by tropical deforestation can be partially initiated by the enhanced energy loss due to the albedo effect.

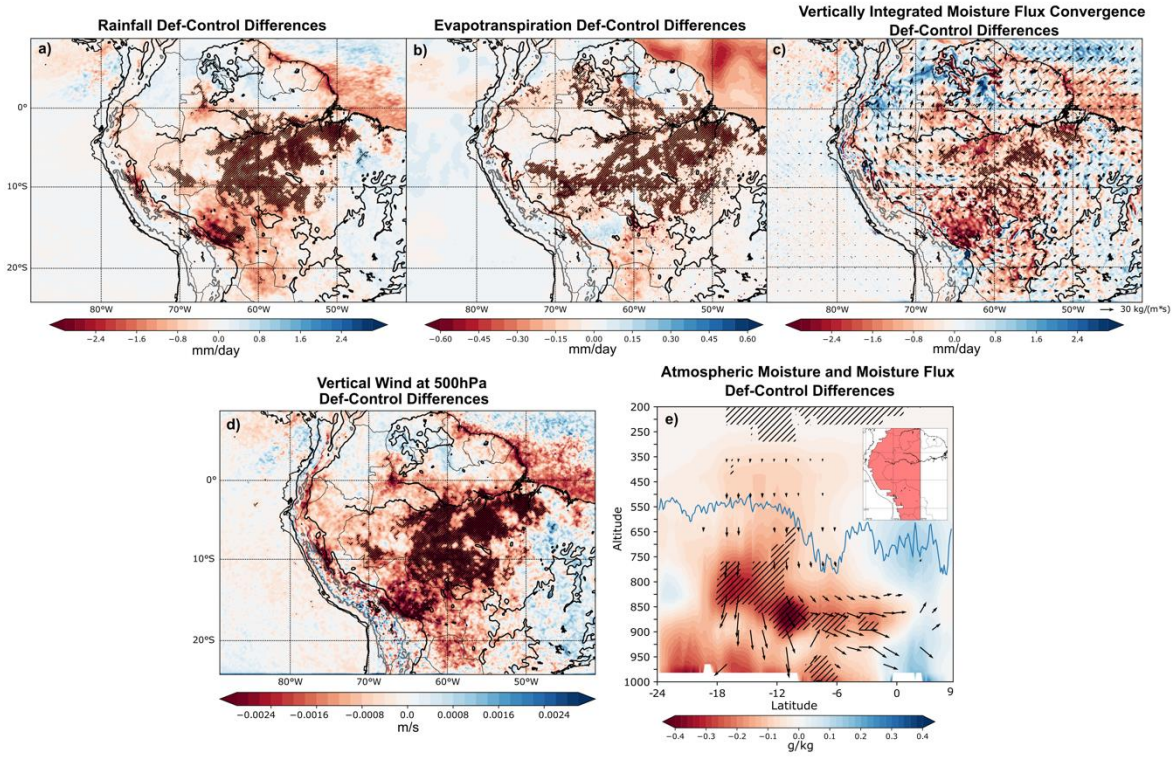

443

444 **Fig 5** DJF seasonal climatological differences Deforested minus Control during 2001-2011 in water balance
445 variables: a) Rainfall ($\Delta\overline{P}_{Def-Con}$). b) Evapotranspiration ($\Delta\overline{E}_{Def-Con}$). c) Vertically integrated moisture flux
446 (vectors) and moisture flux convergence ($-\frac{1}{g}\Delta\nabla\cdot\overline{\int_{1000_{hPa}}^{200_{hPa}} q\,\vec{V}_H dp}_{Def-Con}$;shaded). d) Vertical velocity at 500
447 hPa in m/s. e) Meridional moisture (shaded, in g/kg) and moisture flux (vectors in g/kg*m/s) zonally averaged
448 over the shaded region displayed at the upper right side. Only significant vectors are shown. Figures a-c are in
449 mm/day. Significant changes (t-test, p<0.05) are marked with black slashes. Orography elevation is shown in Figs.
450 5a-d at 500 and 3500 m a.s.l. as black and grey contours, respectively. The blue line in Fig. 5e represents the
451 Andes' profile calculated as the maximum topographic elevation inside the area displayed in red at the upper right
452 side
453
454 On the other hand, Figure 6 shows the differences between Deforested and Control scenarios for the DJF
455 climatology of the atmospheric stability index, as well as its adiabatic dry and diabatic moist process components
456 following Eq. (3). An increment in the equivalent potential temperature and the other terms of the equation (red
457 colors in Fig. 6) indicates an increase in the atmospheric stability and an inhibition tendency of the convective
458 activity. Conversely, a decrease in each term of Eq. (3) (blue colors in Fig. 6) implies a reduction trend in
459 atmospheric stability favoring convection development. A first evident result is that dry adiabatic processes
460 exhibit the tendency to reduce the atmospheric stability over the whole region (Fig. 6b). Although with
461 deforestation the troposphere cools at all levels (not shown), the upper levels exhibit a stronger cooling than
462 middle levels, generating the decrease in potential temperature shown in Figure 6b. This effect is more pronounced
463 over the center of the Brazilian Amazon, near the deforested area. Since the model response in sensible heat flux
464 and surface air temperature is strongly underestimated (section 3.2), the reduction in atmospheric stability due to
465 adiabatic processes could be even greater. On the contrary, changes in wet processes and latent heat release lead

to an increase in the atmospheric stability over the central and western Amazon, including the southern Andes and its eastern foothills (Fig. 6c). It is interesting to highlight that these areas have been recognized to be very sensitive to evapotranspiration upstream of the Amazon basin (Zemp et al. 2017; Staal et al. 2018). Over the northern and eastern parts of the continent, a decrease in atmospheric stability that is related to the enhancement in precipitation and moisture convergence (Fig. 5). Since WRF exhibits an underestimated response in evapotranspiration and latent heat flux to deforestation (section 3.2), the effects in atmospheric stability due to moist diabatic processes could be stronger. Similarly, earlier studies suggested two competing mechanisms as a response of tropical deforestation: (i) a dry atmosphere response linked to warmer surface that increases convergence; (ii) an enhanced divergence leaded by reductions in rainfall and latent heat release (Gill 1980; Lindzen and Nigam 1987; Eltahir and Bras 1993; Eltahir 1996). In summary, our results suggest that the combination of both dry adiabatic and moist (latent heat release) processes produces more stable atmospheric conditions and inhibits precipitation over the western part of the Amazonian basin and the eastern flank of the tropical Andes below the Equator (Fig. 6a). Colombia, Venezuela, Guyana and eastern Brazilian Amazon experience a net reduction in stability and more favorable conditions for convection in the deforested scenario. These alterations are more regional and not limited to deforested areas. Although changes in atmospheric stability are not statistically significant, the 10-year-period analyzed in this work might not be enough for identifying significant differences.

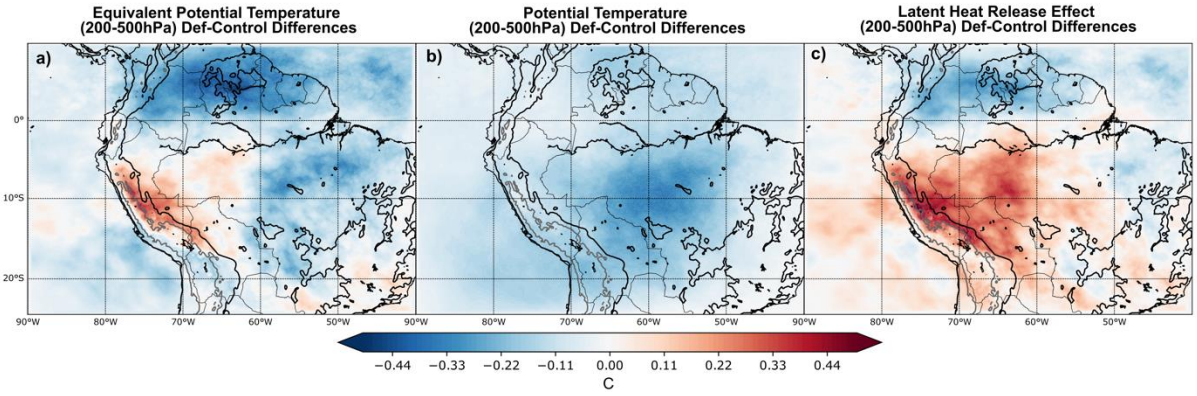

Fig 6 DJF seasonal climatological differences Deforested minus Control during 2001-2011 in atmospheric stability index $\theta_{e_{(200-500)}}$: a) Equivalent potential temperature 200-500 hPa ($\Delta\overline{\theta_{e}}_{200-500_{Def-Con}}$). b) Potential temperature 200-500 hPa ($\Delta\overline{\theta}_{200-500_{Def-Con}}$). c) Latent heat release effect 200-500 hPa ($\Delta\overline{\frac{L_V\theta}{C_PT}r}_{200-500_{Def-Con}}$). All figures are in °C. Orography elevation is shown at 500 and 3500 m a.s.l. as black and grey contours, respectively

4.2 Mesoscale and local changes in daily scale precipitation

The previous section displays how deforestation reduces precipitation and moisture transport, as well as increases the atmospheric stability and inhibits convective activity over the western Amazon and the eastern Andes flank. We analyze the deforestation effect at meso and local scales for daytime and nighttime conditions over the Amazon-Andes transition region, with a particular focus on the Andean valleys of Huarinilla and Zongo in Bolivia (see Figure 1 for precise location).

Daytime and nighttime rainfall patterns are shown in Figure 7 for observations and WRF-D02. During the day, TRMM exhibits high precipitation values over the western part of the Altiplano and Andes highlands (Fig. 7a). Most tropical mountains display this daytime precipitation maximum over summits partially as a result of the thermally driven upslope winds (Garreaud and Wallace 1997; Garreaud 1999; Kikuchi and Wang 2008; Zardi and Whiteman 2013). There are also significant precipitation rates East of the Andes and over Amazonian lowlands during the day as afternoon convection develops (Machado 2002; Romatschke and Houze 2010; Chavez and Takahashi 2017; Fig. 7a). During the night, observed rainfall peaks are located over the eastern Andean piedmonts associated with the so-called rainfall hotspots (Espinoza et al. 2015b; Killeen et al. 2007; Halladay et al. 2012; Fig. 7b). This nocturnal convective activity is driven by the convergence of downslope winds from the top of the Andes with the SALLJ nocturnal enhancement (Killeen et al. 2007; Romatschke and Houze 2010; Chavez and Takahashi 2017; Junquas et al. 2018).

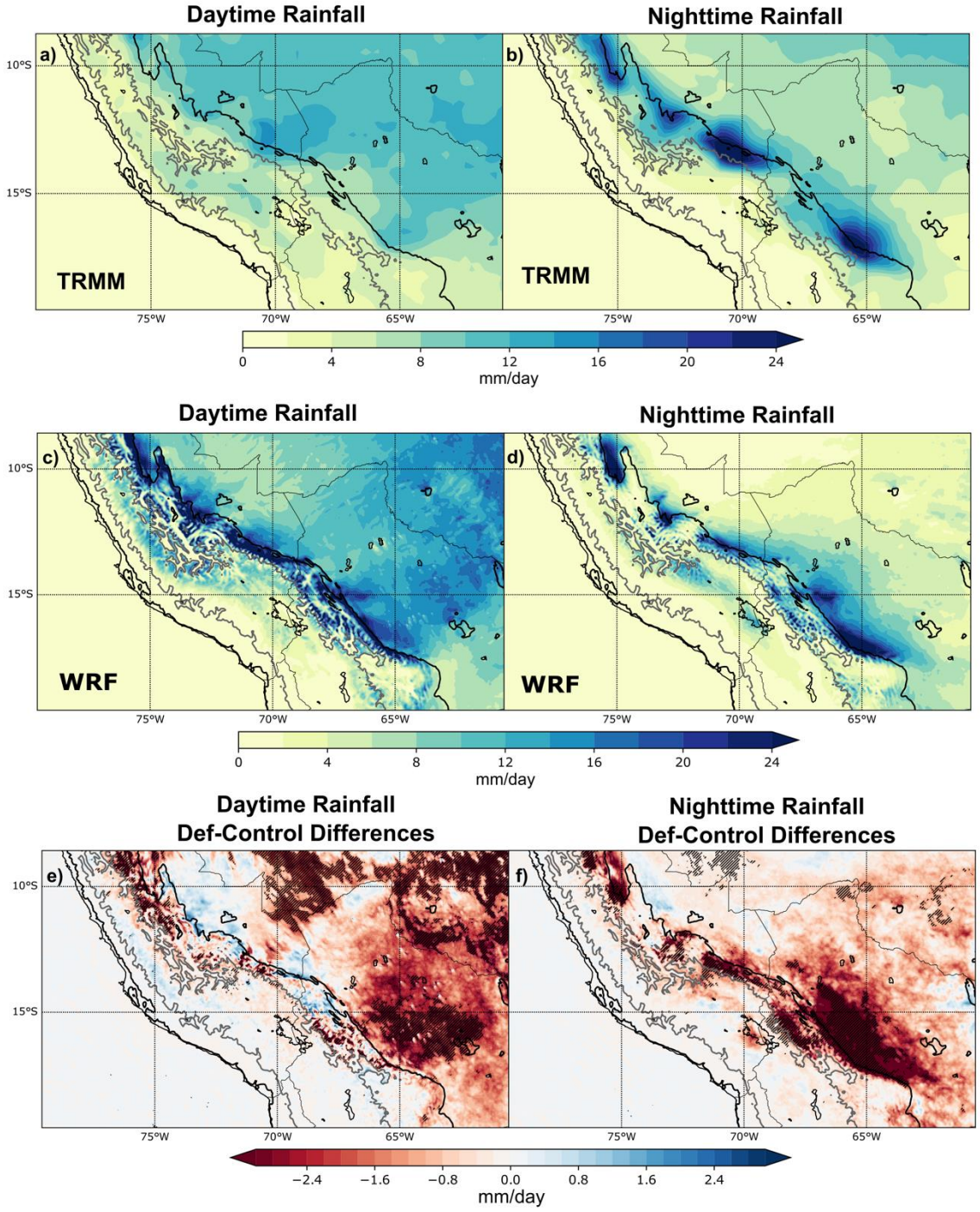

Fig 7 DJF climatological means (2001-2011) for daytime and nighttime precipitation from: a-b) TRMM-3B42. c-d) WRF-D02. e-f) WRF-D02 Deforested-Control differences. All figures are in mm/day. Significant changes (t-test, $p<0.05$) are marked with black slashes. Orography elevation is shown at 500 and 3500 m a.s.l. as black and grey contours, respectively

In general, WRF-D02 is able to represent the main features of diurnal and nocturnal rainfall variability in the region when compared to TRMM. Rainfall peaks above the 3500 m a.s.l. and over the central Peruvian Altiplano are simulated during the day by WRF as shown in Fig. 7c. Daytime convection over Amazon lowlands below 500 m is also present in WRF outputs in agreement with TRMM. However, the model strongly overestimates daytime

519 precipitation over the Bolivian Amazon plains and over the eastern Andes slopes. Nevertheless, dry biases have
520 been identified by several studies in TRMM outputs over tropical Andes, which makes it difficult to properly
521 quantify the model biases (Condom et al. 2011; Scheel et al. 2011; Rasmussen et al. 2013; Espinoza et al. 2015).
522 During nighttime, WRF realistically represents the rainfall hotspots but exhibits a positive (negative) bias over
523 the Peruvian Andes highlands (Brazilian Amazon lowlands) (Fig. 7d).
524
525 Deforestation causes a general rainfall reduction in daytime and nighttime conditions but with different spatial
526 distributions (Figs. 7e-f). During the day, significant precipitation reductions occur over the Amazon plains
527 following the deforested area (between 10-20%), but no significant changes occurs over the tropical Andes above
528 3500m. On the eastern Andean slope between 500 m and 3500 m, significant changes are found, like in the central
529 Andean-Amazon valleys of Peru near the 10°S and 75°W (Fig. 7e). On the other hand, nighttime convection
530 decrease (between 20-30%) is concentrated over the eastern flank of the Andes and particularly over the Bolivian
531 piedmont (Fig. 7f). Taking into account that nighttime convection is responsible for nearly the 70%-80% of the
532 daily precipitation on the eastern tropical Andes slopes during austral summer (Perry et al. 2014; Chavez and
533 Takahashi 2017), this nocturnal rainfall reduction can have a profound impact in the hydrology of the region.
534 Since nocturnal precipitation over the eastern Andes slopes (including over rainfall hotspots) is closely related to
535 the presence of the SALLJ, in Figure 8 we evaluate the changes induced by deforestation in the vertically
536 integrated moisture flux over the Bolivian piedmont inside our third modelling domain (Figure 1). A northwesterly
537 moisture transport is present in both daytime and nighttime conditions during DJF in the Control scenario
538 associated with the SALLJ activity (Fig. 8; e.g. Marengo et al. 2004). This moisture transport is more parallel to
539 the Andes during the day and is stronger and more perpendicular to the slopes during the night in agreement with
540 previous works (Vernekar et al. 2003; Marengo et al. 2004; Junquas et al. 2018; Figs. 8a, b). The humidity flux
541 transported from Amazon toward the Andes is channelized both during day and night over the steepest valleys as
542 modelling and observational works reported in the region (Egger et al. 2005; Perry et al. 2013; Junquas et al. 2018;
543 Figs. 8a, b). The Andes act as a blocking barrier to this moisture laden winds coming from the Amazon lowlands,
544 triggering forced convection mainly during nighttime when the trajectory is more perpendicular to the topography.
545 This mechanism was hypothesized by Espinoza et al. (2015) based on *in-situ* stations and supported by modelling
546 studies (Junquas et al. 2018).
547
548 In the Deforestation scenario, the daytime upslope moisture flux is enhanced over the major valleys (Fig. 8c).
549 However, inside of our region of interest covering Zongo and Huarinilla valleys (black square in Fig. 8) this flux
550 exhibits little changes during the day. Conversely, during the night there is a strong reduction in the humidity
551 transport from the Amazon lowlands toward Andes highlands over the entire region (Fig. 8d) in agreement with
552 nocturnal rainfall reductions over eastern Andes slopes and Bolivian hotspot shown in Figure 7f. By suppressing
553 the condensation latent heating due to rainfall in the Peruvian and Bolivian Andean slopes in a modelling
554 experiment, Junquas et al. (2018) found a similar reduction in the entrance of the upslope moisture flux coming
555 from Amazon plains. A similar scope was assessed by Sun and Barros (2015a, b). Using high resolution climate
556 simulations, they prevent energy entry to the atmosphere from latent heat fluxes over the eastern flank of the
557 Andes in common weather conditions of austral summer and winter. They conclude that the energy available for
558 moist convection is strongly reduced, which is related to less moisture convergence, decreased rainfall and

cloudiness in the region. The upslope flow is also weakened as a consequence of increases in the static stability. Our results points towards the same direction: the crucial role of moist processes for sustaining the atmospheric circulation and hydrological condition over the Amazon-Andes transition region. We hypothesize that, as the atmosphere dries up in our Deforestation scenario and the northerly moisture flux weakens (Fig. 5), a decrease in precipitation starts over the wester Amazon. As rainfall decreases, less latent heat is released to the atmosphere over the region amplifying the precipitation reduction signal. Since latent heating is more important during the night (when sensible heating plays a minor role), major impacts on rainfall occurs.

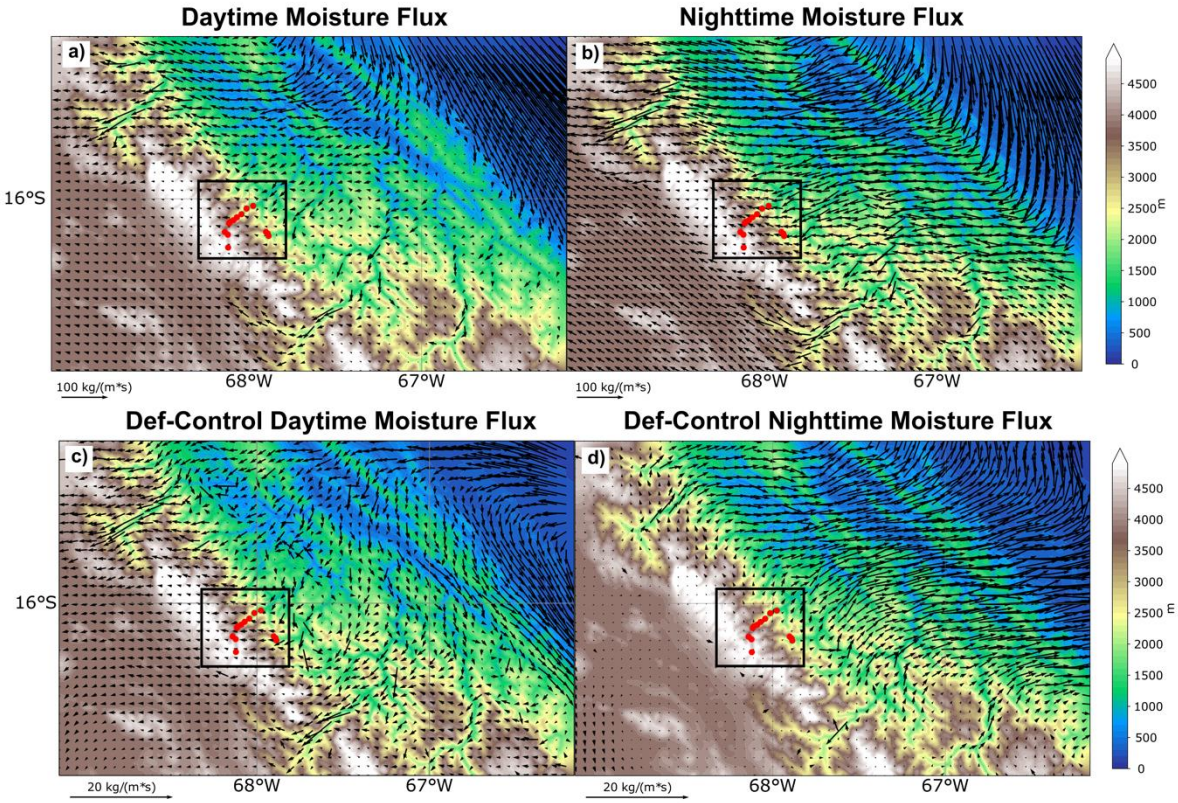

Fig 8 DJF climatological means (2001-2011) for daytime and nighttime vertically-integrated moisture flux from WRF-D03r: a-b) Control and c-d) Deforested minus Control differences. Terrain elevation (shaded) in m and rain-gauge stations (red dots). The black square shows the area where the Andean valleys of Huarinilla and Zongo are located

In order to evaluate the potential impacts of Amazon forest loss in the hydroclimatology at local scales, our analysis is centered in two instrumented valleys located at the eastern flank of the Bolivian Andes: Huarinilla and Zongo Valleys (Fig. 9a). The spatial distribution of rain-gauges within the two valleys allows analyzing how precipitation varies with orography and altitude in two opposite directions with respect to the Andean Cordillera. Stations inside the Zongo Valley are located from north-east to south-west in a perpendicular direction to the Andes (Fig. 9a). Conversely, stations located in the Huarinilla Valley are disposed parallel to the mountain chain. Following the rain stations from highlands to lowlands, two cross-sections were defined as shown in black solid lines of Figure 9a. A third cross-section is analyzed in a perpendicular direction of the Zongo valley (northwest-southeast direction) in order to complement the understanding of local circulation alterations (black dashed line

582 in Fig. 9a). The climatological relationship between precipitation and elevation is shown in Figures 9b-c. There
583 is an opposite relation between rainfall and terrain elevation in the two transects. For Zongo cross-section,
584 precipitation generally decreases with elevation, reaching minimum values above 3000 m a.s.l. and rainfall peaks
585 near the 1000 m a.s.l. (Fig. 9b). This rainfall behavior was previously reported by Espinoza et al (2015). Chavez
586 and Takahashi (2017) demonstrated how the rainfall change with elevation along cross-sections transversal to the
587 Andes in the region follows the profile of the horizontal moisture flux carried by the SALLJ. In this sense, the
588 rainfall-elevation relation in the first transect seems to be more related with synoptic processes such as the SALLJ
589 and less with local upslope processes in accordance with previous studies (Romatschke and Houze 2010). An
590 opposite behavior is observed in Huarinilla Valley, where maximum rainfalls are located at high elevations around
591 3000 m a.s.l. (Fig. 9c). Here, daytime thermally-driven anabatic winds are responsible for transporting moisture
592 transpired inside the valley in the upslope direction and generates a rainfall peak in the afternoon (Molina-Carpio
593 et al. 2019).
594
595 WRF exhibits a realistic representation of the rainfall-elevation relationship for both cross-sections. The model
596 reproduces the observed rainfall increases over very local orographic elevations such as the rain-gauges of
597 Tiquimani, Cahua and Harca. However, a rainfall underestimation (around -30%) occurs in all the stations inside
598 the Zongo Valley and is stronger below the 3000 m a.s.l. Taking into account that precipitation is very related to
599 the SALLJ moisture transport in this valley, WRF rainfall underestimation could be related to the weaker SALLJ
600 moisture flux present in the model simulation (not shown). Daytime and nighttime rainfall conditions for both
601 transects are shown in Figures 9d-g according to WRF outputs. In Zongo Valley, diurnal precipitation is much
602 less than nocturnal values confirming that the dominant mechanism in this valley is the regional moisture transport
603 of the SALLJ (Fig. 9d-f). At this time, precipitation falls mainly over highlands for both transects as shown in
604 Figures 9d-e. Nighttime rainfall is concentrated mainly at lowlands in agreement with the mechanism described
605 before (Fig. 9-f). It is interesting to note that for Huarinilla Valley, similar precipitation magnitudes are simulated
606 for daytime and nighttime conditions (Fig. 9f-g). This suggests that local and synoptic mechanisms are equally
607 important in this valley as reported from previous works (Molina-Carpio et al. 2019).
608
609 Amazon deforestation induces significant reductions in the climatological rainfall mean but increases its
610 interannual variability over both Zongo and Huarinilla cross-sections (Fig. 9b-c). Major precipitation drop is
611 located over areas below 2000 m a.s.l. in the Zongo Valley (Fig. 9b). For this cross-section, daytime precipitation
612 presents little changes in its mean value with a slight reduction (increase) over highlands (lowlands). However,
613 daytime rainfall interannual variability increases in the deforestation scenario (Fig. 9d). Conversely, during the
614 night precipitation decreases, especially at lowlands, but no change in the variability occurs (Fig. 9f). This result
615 confirms our hypothesis that rainfall depletion in this valley is mainly related with the minor entry to SALLJ moist
616 winds from Amazon towards Andes highlands. On the other hand, Huarinilla cross-section does not present
617 significant changes in daytime rainfall (Fig. 9e). However, decreased rainfall and increased variability take place
618 during nighttime especially over highlands in agreement with the regional alterations in the SALLJ related
619 moisture flux (Fig. 9g).
620

Aiming to complement the previous analysis, Figure 10 displays the atmospheric humidity and moisture flux in the vertical cross-section along parallel (black solid line in Fig. 9a) and perpendicular (black dashed line in Fig. 9a) directions of the Zongo Valley. Similar results are found for Huarinilla Valley (not shown). During daytime, upslope moisture flux (Fig. 10a) is causes the rainfall peaks over summits described in Figure 9d. It is interesting to note that the strong ascent around Botijlaca station seems to be related to the maximum in precipitation around this area (Fig. 9d). Similar anabatic winds are present in the perpendicular direction of the Zongo Valley (Fig. 10c). During nighttime, surface moisture flux weakens, and light katabatic winds develops in the Zongo Valley (Fig. 10b-d). At the same time, the mid-tropospheric moisture coming from the Amazon plains is strengthened mainly in the perpendicular direction of the Zongo Valley (Figs. 8a-b, 10b-d). Another interesting feature of the nocturnal circulation in the perpendicular direction is the development of a moisture flux around 700hPa in the opposite direction (northwest-southeast) of the main mid-tropospheric flow (Fig. 10d). This returning flow seems to be a consequence of the ascension motion over lowlands summits to satisfy continuity.

Deforestation induces a weakening of the daytime upslope flow over both directions of the Zongo Valley (Figs. 10e-g). A reduction in the intensity of the daytime circulation increases the atmospheric moisture near the surface at the bottom of the valley and is related to the slight rainfall increase (decrease) over lowlands (highlands) described before (Fig. 9d). Based on the thermodynamic of heat engines, Souza et al. (2000) explain the physical mechanism behind the observed circulation over areas with different surface conditions in sloping terrains. According to this work, the intensity of the circulation depends on the absorption of sensible and latent heat by a parcel that moves along a closed streamline. They also recognize the hydrostatic pressure and nonadiabatic expansion/compression as important effects. Following this argument, we assess the surface energy balance along the Zongo Valley for the Control and Deforestation scenarios. We focus on daytime conditions, when local surface heterogeneities play an important role (Fig. 11). However, nighttime changes were also analyzed and are not significant (not shown). Small changes in the incoming shortwave radiation are induced by deforestations in the Zongo Valley and are linked with differences in clouds (Fig. 11a). On the contrary, a strong increment in the reflected shortwave radiation causes a lost of around -40W/m^2 at the bottom of the valley where deforestation occurs (Fig. 11b). The longwave components of the energy balance remain almost unaltered (Figs. 11c-d). Due to the increase in the outgoing shortwave energy loss, the surface net radiation decreases at lowlands below Chururaqui rain-gauge (Fig. 11e). This net radiation reduction generates a decrease in the altitude of the planetary boundary layer (PBL) (Fig.11f) and is distributed in reductions in latent heat but mainly in sensible heat flux over lowlands (Fig. 11g-h). These fluxes are essential in the triggering and development of upslope flows (e.g., Junquas et al 2018). The reductions in the sensible and latent heat fluxes explain the weakening of the upslope surface circulation during daytime described in Figure 10.

On the other hand, nighttime differences in circulation mainly occur at regional scale through mid-tropospheric moisture flux reduction in the deforested scenario (Figs. 8d, 10f-h). This moisture transport is very important for developing the nocturnal convection and its decrease causes less rainfall over the entire region (Fig. 9f-g). The nighttime conditions are also characterized by a strong reduction in atmospheric humidity above the 600hPa as a consequence of deforestation (Fig. 10f-h).

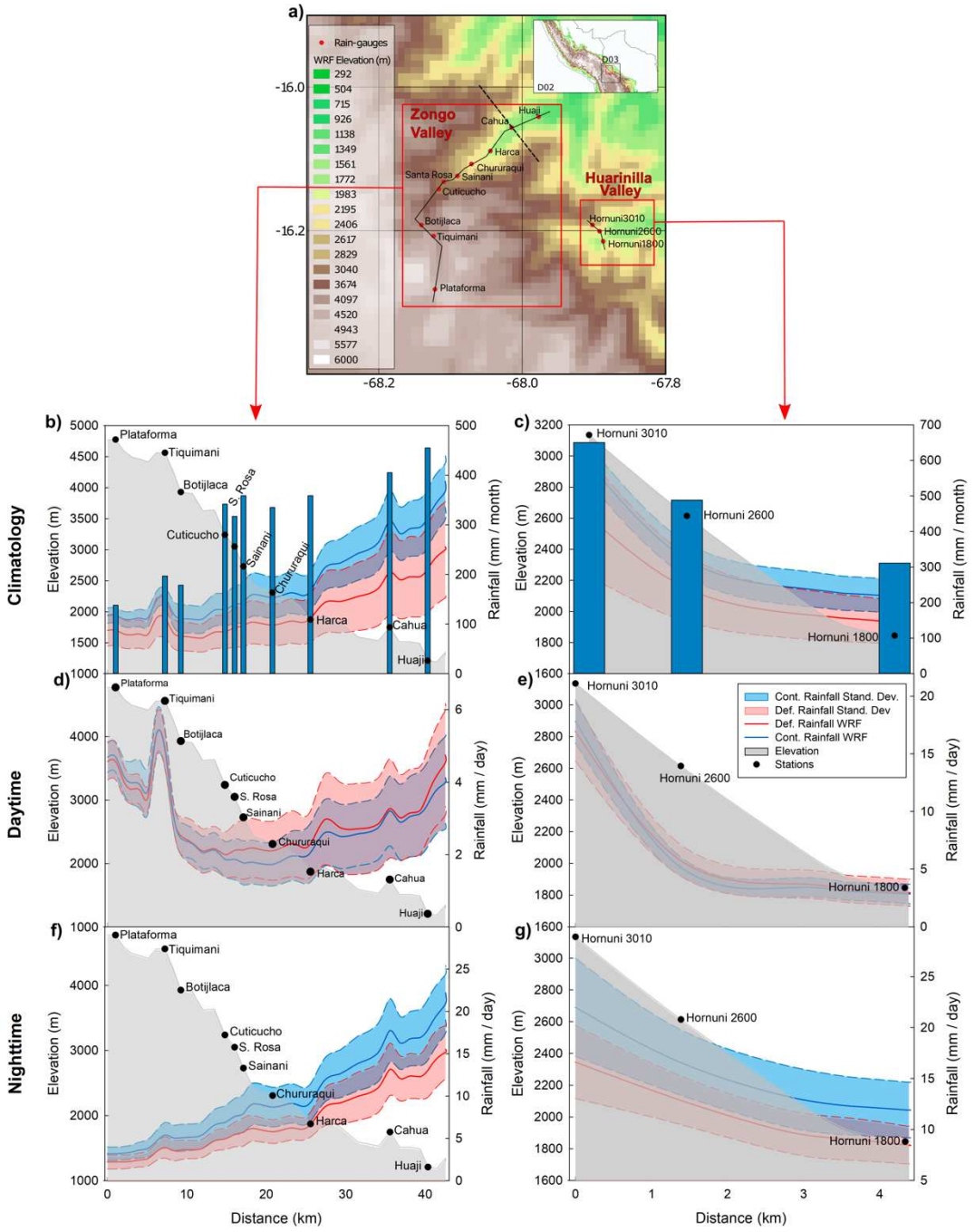

Fig 9 a) Map of the subregion inside D03 with terrain elevation (shaded) in m and rain-gauge stations (red dots). Two selected cross-sections are indicated in black solid lines. A perpendicular cross-section in Zongo Valley shown in Figure 10 is indicated as a dashed black line. b-c) Cross-sections for b) Zongo Valley and c) Huarinilla Valley. Topographical profiles are displayed as a gray line (in m). Observed rain-gauge rainfall is presented as blue bars. WRF-D03 Control and Deforested rainfall climatological means are shown as blue and red lines and are labeled as Cont. and Def., respectively. Rainfall is in mm/month. d-g) Same as Fig. 9b-c but for daytime and nighttime conditions. Rainfall is in mm/day. The x axis represents the horizontal distance in km along the cross-sections. Blue and red envelopes represent model standard deviation for each scenario. Black dots represent rain-gauge stations

672
673 Rainfall reductions and increased rainfall variability over Huarinilla and Zongo Valleys can impact the wet
674 ecosystems of local humid-montane forest and its endemic biological species (Ibisch et al. 2001; Mueller et al.
675 2002; Kessler and Kluge 2008). Additionally, the area encompasses part of the Cordillera Real-Bolivia and the
676 Huayna Potosi Massif where several glaciers (e.g. Zongo Glacier) are located (Francou et al. 1995). The surface
677 glacier mass balance variability of the tropical glaciers is strongly controlled by the precipitation amount and
678 temporal distribution that determine the glacier surface albedo and therefore the surface energy balance (e.g. Sicart
679 et al. 2005; Rabatel et al. 2013), as well as regional atmospheric circulation (Favier 2004; Sicart et al. 2016). Our
680 results state that Amazonian large-scale deforestation can have an important effect in the regional circulation and
681 precipitation. This means that retreat of the tropical Andes glacier documented since the early 1980s and linked
682 to climate change (e.g. Ramírez et al. 2001; Francou et al. 2003; Rabatel etl al. 2013) is likely to be further
683 increased as extensive Amazonian deforestation can also have an impact on precipitation and therefore on the
684 surface mass balance of tropical glaciers.
685

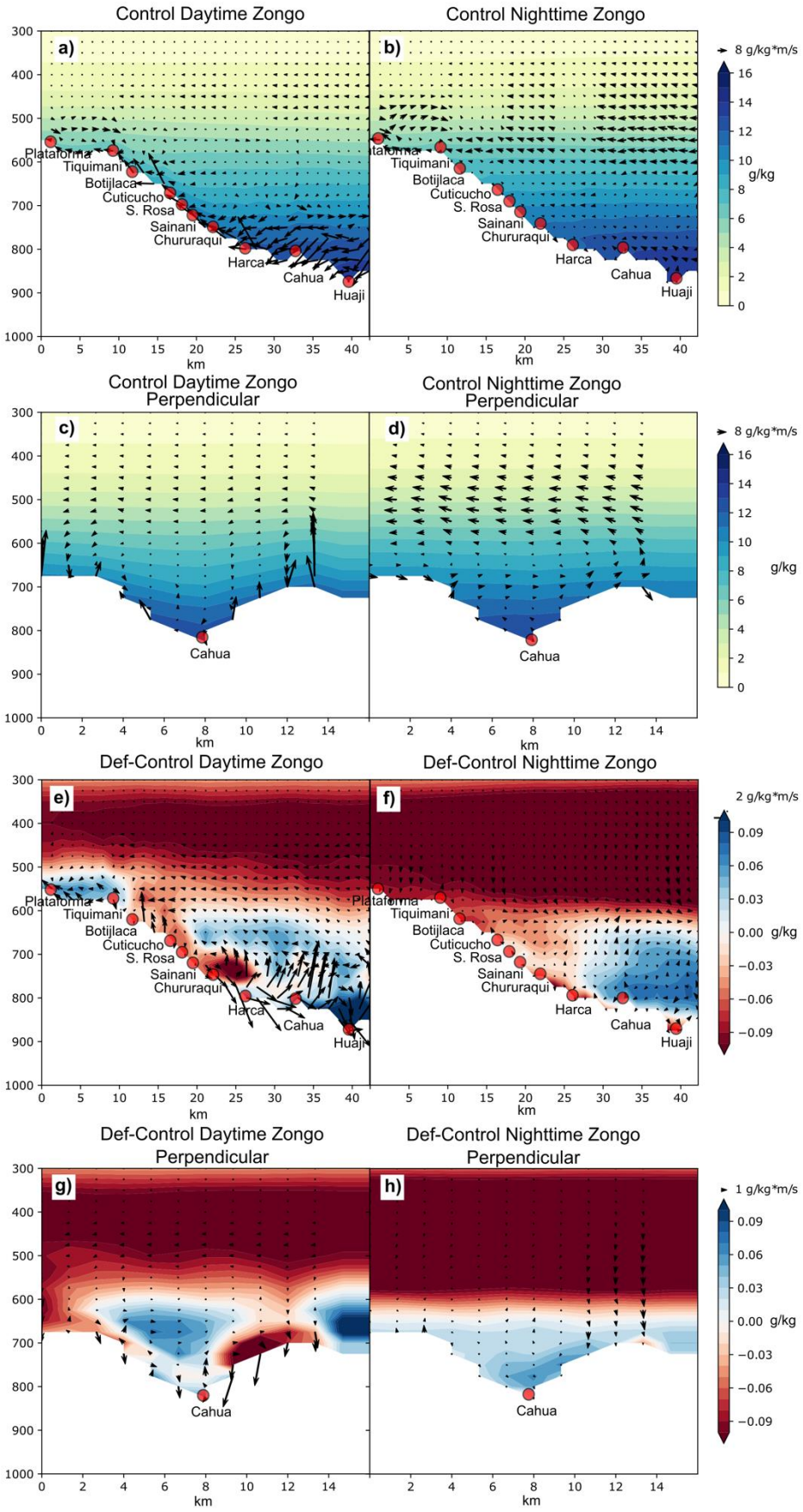

Fig 10 Vertical cross-section for daytime and nighttime DJF climatological means (2001-2011) in atmospheric moisture (shaded, g/kg) and moisture flux (vectors, g/kg*m/s) for the Zongo Valley in two opposite directions:

parallel to the transect (see black solid line in Fig. 9a) and perpendicular to the transect (see black dashed line in Fig. 9a). Daytime (a) and nighttime (b) WRF-Control conditions for the transect parallel to the Zongo Valley. Daytime (c) and nighttime (d) WRF-Control conditions for the transect perpendicular to the Zongo Valley. Daytime (e) and nighttime (f) Deforested minus Control differences in the transect parallel to the Zongo Valley. Daytime (g) and nighttime (h) Deforested minus Control differences in the transect perpendicular to the Zongo Valley. Red dots represent rain-gauge stations. Vertical component of the moisture flux is exaggerated by a factor of ten

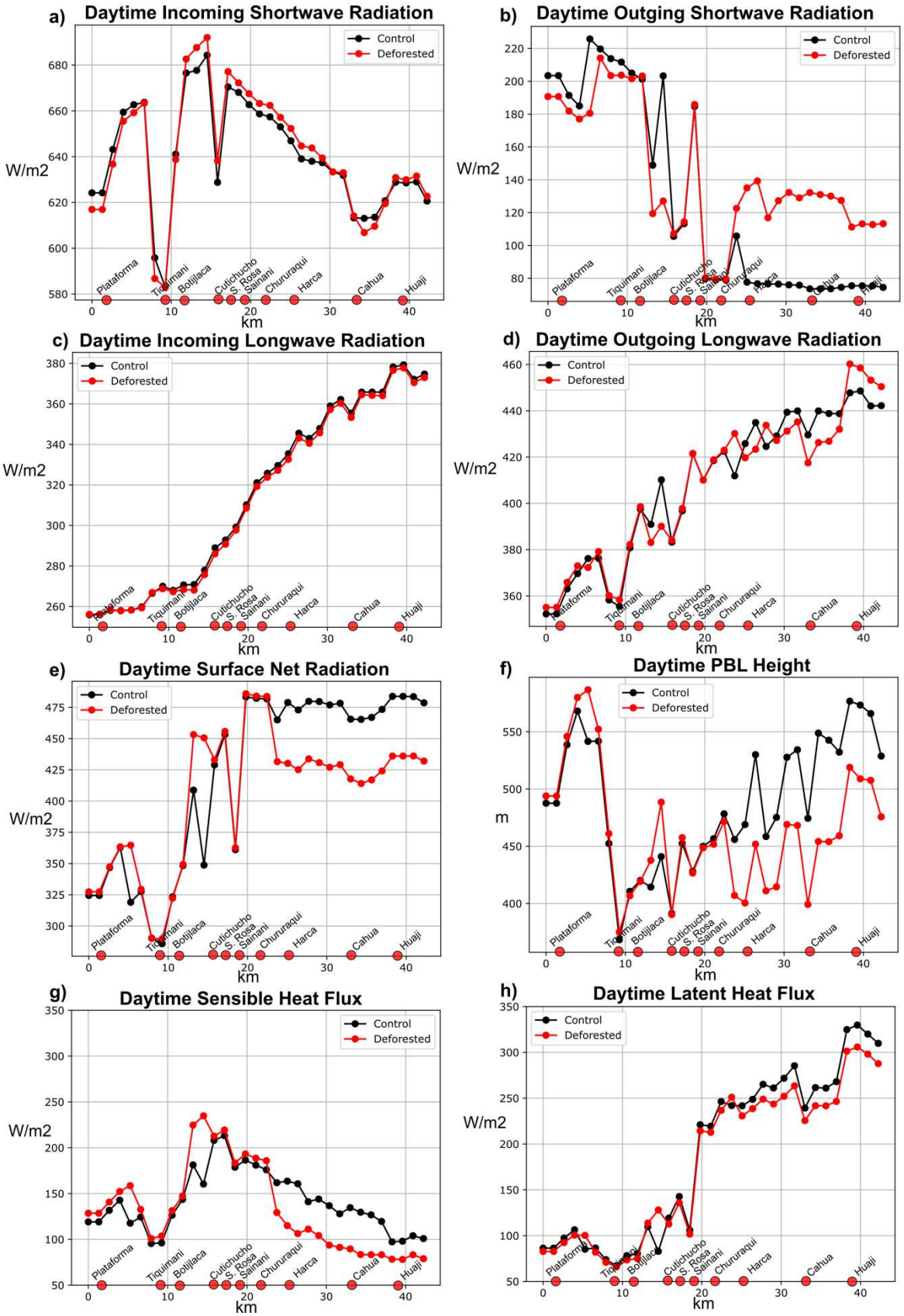

Fig 11 WRF-D03 daytime mean variation along the Zongo Valley transect in Control and Deforested scenarios (black and red lines, respectively) for: a) Shortwave incoming radiation. b) Shortwave outgoing radiation. c)

Longwave incoming radiation. d) Longwave outgoing radiation. e) Surface net radiation. f) Planetary boundary layer (PBL) height. g) Sensible heat flux. h) Latent heat flux. Red dots represent rain-gauge stations

It is important to remark that spread deforestation can have strong nonlocal atmospheric responses (Avissar and Werth 2005; Hasler et al. 2009). Thus, the use of a regional model where both control and deforested scenarios present the same lateral boundary conditions generates a bias where these nonlocal effects are not included (Medvigy et al. 2011). In this sense, the results discussed above do not include the possible remote responses of deforestation in the boundary conditions of our analysis domain.

5. Summary and conclusions

This study aims to evaluate the impacts of Amazonian deforestation in the hydro-climatic connectivity between Amazon and eastern tropical Andes during the austral summer in terms of hydrological and energetic balances. To this end, we use 10-year December-January-February high-resolution simulations (2001-2011) with the regional climate model WRF. Two scenarios are used: (i) a control simulation corresponding to vegetation conditions for the year 2000; (ii) a business-as-usual deforested scenario (45% of forest lost) designed by Soares-Filho et al. (2006).

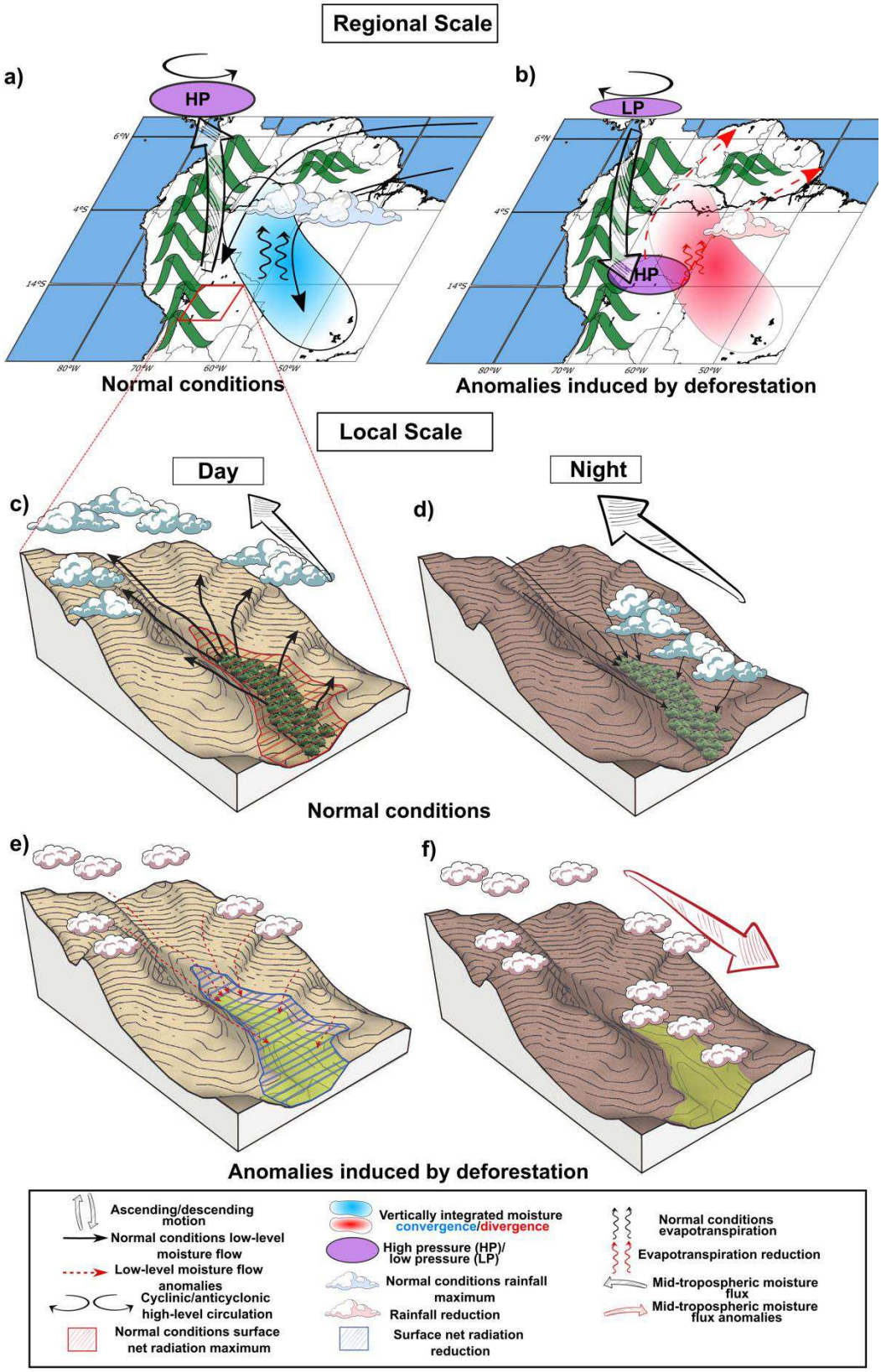

Fig 12 Schematic representation of DJF climatological atmospheric conditions at regional (a-b) and local scales (c-f) for normal conditions (a-c-d) and deforestation induced anomalies (b-e-f) in WRF simulations. The red square in a indicates the approximated location of the Zongo Valley sketched in c-f. Black solid (red dashed) thin arrows represent surface moisture transport under normal conditions (deforestation anomalies). Black (red) thick

arrows represent mid-tropospheric moisture flux under normal conditions (deforestation anomalies). Vertical thick arrows represent ascending and descending motions. Black (red) curved arrows represent evapotranspiration under normal conditions (deforestation anomalies). Blue and red shaded areas indicate vertically integrated moisture convergence and divergence, respectively. Purple areas indicate pressure changes. Blue and red clouds indicate rainfall maximum and rainfall reductions under normal and deforested conditions, respectively. Red (blue) hatched area in c (e) indicates surface net radiation maximum (reduction) under normal (deforestation) conditions

By comparing with reanalysis (ERA5) and precipitation satellite outputs (TRMM), we find a realistic representation of the main atmospheric circulation (e.g. SALLJ, the Bolivian High) and rainfall features (e.g. SACZ, Amazon convection) during austral summer by WRF at a regional scale. The model is also able to reproduce the daytime and nighttime rainfall conditions over the Amazon-Andes transition region and the rainfall-elevation relation at a local-scales inside instrumented Andean valleys. However, at local scale, in regions with high orography, day and night rainfall conditions were only compared with rain-gauge estimations for a very short period (one year) in Huarinilla valley. The lack of observations at intra-diurnal time scale in the region is an important limitation for assessing the high-resolution model representation of local atmospheric mechanisms and its interaction with mesoscale features. We complement the validation by assessing the model skill to reproduce the observed land use change impacts in surface fluxes and atmospheric variables at a local scale against LBA stations. We find a realistic model response to deforestation for most of the surface atmospheric variables in Amazon lowlands. However, WRF overestimates the effect of the albedo on the reflected shortwave radiation and strongly underestimates the sensible heat flux and evaporation/latent heat response to forest loss. These model biases constrain our conclusions about the impacts of deforestation on the regional climate. How these errors interact with each other is something that remains unexplored in this work.

At a regional scale, the energy balance is profoundly disrupted by the forest loss. The combined effect of enhanced energy losses through shortwave radiation reflection, longwave incoming and outgoing radiation fluxes leads to a decrease in the surface net radiation over most of the basin. According to the deforestation theory developed by Zeng and Neeling (1998), this reduction in surface net radiation may lead to alterations in the regional moisture convergence. Accordingly, deforestation reduces precipitation almost over the entire Amazonian basin (~20%). Rainfall depletion is related with the very local response of decreased evapotranspiration over cleared areas. The drier atmosphere seems to present a decrease in latent heat release that weakens moisture convergence and causes an anomalous winds subsidence in the region in agreement with early theoretical frameworks. In agreement with these theoretical works, deforestation induces a slight weakening of the Bolivian High and decreases (increases) the 200hPa geopotential height (surface pressure) over the southwestern Amazon. These alterations in the regional precipitation and atmospheric circulation are summarized in Figures 12a-b. Regarding the regional atmospheric stability, our analysis suggests the rise of two competing mechanisms for tropical deforestation: (i) an adiabatic response decreases atmospheric stability and enhances convective activity over the continental area; (ii) conversely, reductions in the latent heat release increase atmospheric stability and disfavor convection mainly over western Amazon, and the eastern sides of tropical Andes. Although the effects of deforestation in atmospheric

stability are relatively small and non-significant, the underestimated WRF response in sensible and latent heat fluxes and surface air temperature to forest loss implies that these effects could be stronger.

Over the Amazon-Andes transition region, deforestation causes a general rainfall reduction in both daytime and nighttime conditions but with a clearly spatial differentiation. Daytime precipitation reductions occur over the Amazon plains following the deforested area (between 10-20%). Conversely, nighttime convection decreases between 20-30% mainly over the eastern flank of the Andes and over the Bolivian piedmont. Since nighttime convection is responsible for nearly the 70%-80% of the daily precipitation on the eastern tropical Andes slopes during austral summer, this rainfall reduction can seriously impact the hydrology of the region. The decreasing in nocturnal rainfall over eastern Andean hillside is caused by a reduction in the humidity transport from the Amazon lowlands toward Andes highlands during nighttime in agreement with previous modelling studies.

Finally, at a local scale, Amazon deforestation induces significant reductions in the climatological rainfall mean over both Zongo and Huarinilla valleys (-25%) and increases its interannual variability. For the Zongo Valley, major precipitation drop occurs over areas below 2000 m a.s.l. In this cross-section, daytime precipitation presents little changes in its mean value, with a small increase (decrease) at lowlands (highlands) as a consequence of the weakening of the thermally-driven anabatic circulation (Figs. 12c-e). However, during the night precipitation decreases, especially at lowlands. The rainfall depletion in this valley seems to be mainly related with the minor entry to SALLJ moist winds from Amazon towards Andes highlands (Figs. 12d-f). Similarly, Huarinilla cross-section does not present significant changes in daytime rainfall but exhibits decreased precipitation especially over highlands. However, as a result of numerical modelling these conclusions have to be taken with caution as they are partially dependent on the model configuration. More efforts have to be done to understand the sensitivity and robustness of these results to model parametrizations. Finally, this work and most of deforestation modelling studies are focused on forest loss impacts on atmospheric processes at climatological time scales. How deforestation can alter rainfall distribution and the atmospheric circulation patterns that drives moisture advection at synoptic intra-seasonal time scale is a question that should be addressed to better understand the deforestation disturbances at longer time scales.

Acknowledgments

This research has been supported by the French AMANECER-MOPGA project funded by ANR and IRD (ref. ANR-18-MPGA-0008). Jorge Molina-Carpio was supported by the Universidad Mayor de San Andres (UMSA) within the framework provided by the PHYBAAM (Processus Hydrologiques des Bassins Andins Amazoniens) Project and HYdrogéochimie du Bassin AMazonien (HYBAM) program. We would like to thank Marcus Schawe for providing the rain-gauge data for Hornuni Valley.

Declarations

Funding: This research has been supported by the French AMANECER-MOPGA project funded by ANR and IRD (ref. ANR-18-MPGA-0008). Jorge Molina-Carpio was supported by the Universidad Mayor de San Andres

(UMSA) within the framework provided by the PHYBAAM (Processus Hydrologiques des Bassins Andins Amazoniens) Project and HYdrogéochimie du Bassin AMazonien (HYBAM) program. We would like to thank Marcus Schawe for providing the rain-gauge data for Hornuni Valley.

Conflicts of interest/Competing interests: The authors declare no conflicts of interest or competing interests.

Availability of data and material: All dataset sources except WRF modelling results have been properly referenced by showing the source (web site links). The datasets generated during the current study (WRF outputs) are available from the corresponding author on reasonable request

Author contributions: All authors contributed to the study conception and design. Material preparation, data collection and analysis were performed by Juan P. Sierra. The first draft of the manuscript was written by Juan P. Sierra and all authors commented on previous versions of the manuscript. All authors read and approved the final manuscript.

References

Alves LM, Marengo JA, Fu R, Bombardi RJ (2017) Sensitivity of Amazon Regional Climate to Deforestation. Am J Clim Chang. https://doi.org/10.4236/ajcc.2017.61005

Armijos E, Crave A, Espinoza JC, et al (2020) Rainfall control on Amazon sediment flux: synthesis from 20 years of monitoring. Environ Res Commun 2:051008. https://doi.org/10.1088/2515-7620/ab9003

Atkinson BW (1989) Meso-scale atmospheric circulations

Avissar R, Schmidt T (1998) An Evaluation of the Scale at which Ground-Surface Heat Flux Patchiness Affects the Convective Boundary Layer Using Large-Eddy Simulations. J Atmos Sci 55:2666–2689. https://doi.org/10.1175/1520-0469(1998)055<2666:AEOTSA>2.0.CO;2

Avissar R, Werth D (2005) Global Hydroclimatological Teleconnections Resulting from Tropical Deforestation. J Hydrometeorol 6:134–145. https://doi.org/10.1175/JHM406.1

Badger AM, Dirmeyer PA (2015) Climate response to Amazon forest replacement by heterogeneous crop cover. Hydrol Earth Syst Sci 19:4547–4557. https://doi.org/10.5194/hess-19-4547-2015

Bagley JE, Desai AR, Harding KJ, et al (2014) Drought and deforestation: Has land cover change influenced recent precipitation extremes in the Amazon? J Clim 27:345–361. https://doi.org/10.1175/JCLI-D-12-00369.1

Bala G, Caldeira K, Wickett M, et al (2007) Combined climate and carbon-cycle effects of large-scale deforestation. Proc Natl Acad Sci U S A 104:6550–6555. https://doi.org/10.1073/pnas.0608998104

Bastable HG, Shuttleworth WJ, Dallarosa RLG, et al (1993) Observations of climate, albedo, and surface radiation over cleared and undisturbed amazonian forest. Int J Climatol. https://doi.org/10.1002/joc.3370130706

Berbet MLC, Costa MH (2003) Climate Change after Tropical Deforestation: Seasonal Variability of Surface Albedo and Its Effects on Precipitation Change. J Clim 16:2099–2104. https://doi.org/10.1175/1520-0442(2003)016<2099:CCATDS>2.0.CO;2

Boers N, Marwan N, Barbosa HMJ, Kurths J (2017) A deforestation-induced tipping point for the South American monsoon system. Sci Rep. https://doi.org/10.1038/srep41489

Bonan GB (2008) Forests and Climate Change: Forcings, Feedbacks, and the Climate Benefits of Forests. Science (80-) 320:1444–1449. https://doi.org/10.1126/science.1155121

Brockhaus P, Lüthi D, Schär C (2008) Aspects of the diurnal cycle in a regional climate model. Meteorol Zeitschrift 17:433–443. https://doi.org/10.1127/0941-2948/2008/0316

Brubaker KL, Entekhabi D, Eagleson PS (1993) Estimation of Continental Precipitation Recycling. J Clim 6:1077–1089. https://doi.org/10.1175/1520-0442(1993)006<1077:EOCPR>2.0.CO;2

Butt N, De Oliveira PA, Costa MH (2011) Evidence that deforestation affects the onset of the rainy season in Rondonia, Brazil. J Geophys Res Atmos. https://doi.org/10.1029/2010JD015174

Chavez SP, Takahashi K (2017) Orographic rainfall hot spots in the Andes-Amazon transition according to the TRMM precipitation radar and in situ data. J Geophys Res. https://doi.org/10.1002/2016JD026282

Chen F, Avissar R (1994) Impact of Land-Surface Moisture Variability on Local Shallow Convective Cumulus

852 and Precipitation in Large-Scale Models. J Appl Meteorol 33:1382–1401. https://doi.org/10.1175/1520-
853 0450(1994)033<1382:IOLSMV>2.0.CO;2
854 Chen F, Dudhia J (2001) Coupling an Advanced Land Surface–Hydrology Model with the Penn State–NCAR
855 MM5 Modeling System. Part I: Model Implementation and Sensitivity. Mon Weather Rev 129:569–585.
856 https://doi.org/10.1175/1520-0493(2001)129<0569:CAALSH>2.0.CO;2
857 Claussen M, Brovkin V, Ganopolski A (2001) Biophysical versus biogeochemical feedbacks of large-scale land
858 cover change. Geophys Res Lett. https://doi.org/10.1029/2000GL012471
859 Condom T, Rau P, Espinoza JC (2011) Correction of TRMM 3B43 monthly precipitation data over the
860 mountainous areas of Peru during the period 1998-2007. Hydrol Process 25:1924–1933.
861 https://doi.org/10.1002/hyp.7949
862 Correia FWS, Alvalá RCS, Manzi AO (2008) Modeling the impacts of land cover change in Amazonia: a
863 regional climate model (RCM) simulation study. Theor Appl Climatol 93:225–244.
864 https://doi.org/10.1007/s00704-007-0335-z
865 Costa MH, Pires GF (2010) Effects of Amazon and Central Brazil deforestation scenarios on the duration of the
866 dry season in the arc of deforestation. Int J Climatol 30:1970–1979. https://doi.org/10.1002/joc.2048
867 D'Almeida C, Vörösmarty CJ, Hurtt GC, et al (2007) The effects of deforestation on the hydrological cycle in
868 Amazonia: A review on scale and resolution. Int. J. Climatol.
869 Dalu GA, Pielke RA (1993) Vertical Heat Fluxes Generated by Mesoscale Atmospheric Flow Induced by
870 Thermal Inhomogeneities in the PBL. J Atmos Sci 50:919–926. https://doi.org/10.1175/1520-
871 0469(1993)050<0919:VHFGBM>2.0.CO;2
872 De Noblet-Ducoudré N, Boisier JP, Pitman A, et al (2012) Determining robust impacts of land-use-induced land
873 cover changes on surface climate over North America and Eurasia: Results from the first set of LUCID
874 experiments. J Clim. https://doi.org/10.1175/JCLI-D-11-00338.1
875 Debortoli NS, Dubreuil V, Hirota M, et al (2017) Detecting deforestation impacts in Southern Amazonia rainfall
876 using rain gauges. Int J Climatol. https://doi.org/10.1002/joc.4886
877 Dirmeyer PA, Brubaker KL (2007) Characterization of the global hydrologic cycle from a back-trajectory
878 analysis of atmospheric water vapor. J Hydrometeorol. https://doi.org/10.1175/JHM557.1
879 Dudhia J (1989) Numerical Study of Convection Observed during the Winter Monsoon Experiment Using a
880 Mesoscale Two-Dimensional Model. J Atmos Sci 46:3077–3107. https://doi.org/10.1175/1520-
881 0469(1989)046<3077:NSOCOD>2.0.CO;2
882 Duveiller G, Hooker J, Cescatti A (2018) The mark of vegetation change on Earth's surface energy balance. Nat
883 Commun 9:679. https://doi.org/10.1038/s41467-017-02810-8
884 Egger J, Blacutt L, Ghezzi F, et al (2005) Diurnal Circulation of the Bolivian Altiplano. Part I: Observations.
885 Mon Weather Rev 133:911–924. https://doi.org/10.1175/MWR2894.1
886 Eiras-Barca J, Dominguez F, Yang Z, et al (2020) Changes in South American hydroclimate under projected
887 Amazonian deforestation. Ann N Y Acad Sci. https://doi.org/10.1111/nyas.14364
888 Eltahir EAB (1996) Role of vegetation in sustaining large-scale atmospheric circulations in the tropics. J
889 Geophys Res Atmos 101:4255–4268. https://doi.org/10.1029/95JD03632
890 Eltahir EAB, Bras RL (1993) On the response of the tropical atmosphere tio large-scale deforestation. Q J R
891 Meteorol Soc 119:779–793. https://doi.org/10.1002/qj.49711951209
892 Eltahir EAB, Bras RL (1994) Precipitation recycling in the Amazon basin. Q J R Meteorol Soc.
893 https://doi.org/10.1002/qj.49712051806
894 Espinoza JC, Chavez S, Ronchail J, et al (2015) Rainfall hotspots over the southern tropical Andes: Spatial
895 distribution, rainfall intensity, and relations with large-scale atmospheric circulation. Water Resour Res.
896 https://doi.org/10.1002/2014WR016273
897 Espinoza JC, Marengo JA, Ronchail J, et al (2014) The extreme 2014 flood in south-western Amazon basin:
898 The role of tropical-subtropical South Atlantic SST gradient. Environ Res Lett 9:124007.
899 https://doi.org/10.1088/1748-9326/9/12/124007
900 Espinoza JC, Ronchail J, Marengo JA, Segura H (2019a) Contrasting North–South changes in Amazon wet-day
901 and dry-day frequency and related atmospheric features (1981–2017). Clim Dyn.
902 https://doi.org/10.1007/s00382-018-4462-2
903 Espinoza JC, Sörensson AA, Ronchail J, et al (2019b) Regional hydro-climatic changes in the Southern Amazon
904 Basin (Upper Madeira Basin) during the 1982–2017 period. J Hydrol Reg Stud 26:100637.
905 https://doi.org/10.1016/j.ejrh.2019.100637
906 Espinoza Villar JC, Ronchail J, Guyot JL, et al (2009) Spatio-temporal rainfall variability in the Amazon basin
907 countries (Brazil, Peru, Bolivia, Colombia, and Ecuador). Int J Climatol 29:1574–1594.
908 https://doi.org/10.1002/joc.1791
909 Eva HD, Belward AS, De Miranda EE, et al (2004) A land cover map of South America. Glob Chang Biol
910 10:731–744. https://doi.org/10.1111/j.1529-8817.2003.00774.x
911 Favier V (2004) One-year measurements of surface heat budget on the ablation zone of Antizana Glacier 15,

912 Ecuadorian Andes. J Geophys Res 109:D18105. https://doi.org/10.1029/2003JD004359
913 Fearnside PM (1993) Deforestation in Brazilian Amazonia: The effect of population and land tenure. Ambio.
914 https://doi.org/10.1016/0006-3207(94)90222-4
915 Figueroa SN, Satyamurty P, Da Silva Dias PL (1995) Simulations of the Summer Circulation over the South
916 American Region with an Eta Coordinate Model. J Atmos Sci 52:1573–1584.
917 https://doi.org/10.1175/1520-0469(1995)052<1573:SOTSCO>2.0.CO;2
918 Fisher JB, Whittaker RJ, Malhi Y (2011) ET come home: Potential evapotranspiration in geographical ecology.
919 Glob. Ecol. Biogeogr.
920 Francou B, Ribstein P, Saravia R, Tiriau E (1995) Monthly balance and water discharge of an inter-tropical
921 glacier: Zongo Glacier, Cordillera Real, Bolivia, 16° S. J Glaciol 41:61–67.
922 https://doi.org/10.3189/S0022143000017767
923 Francou B, Vuille M, Wagnon P, et al (2003) Tropical climate change recorded by a glacier in the central Andes
924 during the last decades of the twentieth century: Chacaltaya, Bolivia, 16°S. J Geophys Res 108:4154.
925 https://doi.org/10.1029/2002JD002959
926 Fu R, Li W (2004) The influence of the land surface on the transition from dry to wet season in Amazonia.
927 Theor Appl Climatol. https://doi.org/10.1007/s00704-004-0046-7
928 Fu R, Yin L, Li W, et al (2013) Increased dry-season length over southern Amazonia in recent decades and its
929 implication for future climate projection. Proc Natl Acad Sci U S A.
930 https://doi.org/10.1073/pnas.1302584110
931 Garreaud R (1999) Multiscale Analysis of the Summertime Precipitation over the Central Andes. Mon Weather
932 Rev 127:901–921. https://doi.org/10.1175/1520-0493(1999)127<0901:MAOTSP>2.0.CO;2
933 Garreaud R, Wallace JM (1997) The Diurnal March of Convective Cloudiness over the Americas. Mon Weather
934 Rev 125:3157–3171. https://doi.org/10.1175/1520-0493(1997)125<3157:TDMOCC>2.0.CO;2
935 Gash JHC, Nobre CA (1997) Climatic Effects of Amazonian Deforestation: Some Results from ABRACOS.
936 Bull Am Meteorol Soc 78:823–830. https://doi.org/10.1175/1520-
937 0477(1997)078<0823:CEOADS>2.0.CO;2
938 Gash JHC, Shuttleworth WJ (1991) Tropical deforestation: Albedo and the surface-energy balance. Clim
939 Change 19:123–133. https://doi.org/10.1007/BF00142219
940 Gedney N, Valdes PJ (2000) The effect of Amazonian deforestation on the northern hemisphere circulation and
941 climate. Geophys Res Lett. https://doi.org/10.1029/2000GL011794
942 Gill AE (1980) Some simple solutions for heat-induced tropical circulation. Q. J. R. Meteorol. Soc. 106:447–
943 462
944 Grell GA, Dévényi D (2002) A generalized approach to parameterizing convection combining ensemble and
945 data assimilation techniques. Geophys Res Lett 29:38-1-38–4. https://doi.org/10.1029/2002GL015311
946 Halladay K, Malhi Y, New M (2012) Cloud frequency climatology at the Andes/Amazon transition: 2. Trends
947 and variability. J Geophys Res Atmos 117:n/a-n/a. https://doi.org/10.1029/2012JD017789
948 Hartmann DL, Klein Tank AMG, Rusticucci M, et al (2013) Observations: Atmosphere and surface. In: Climate
949 Change 2013 the Physical Science Basis: Working Group I Contribution to the Fifth Assessment Report
950 of the Intergovernmental Panel on Climate Change
951 Hasler N, Werth D, Avissar R (2009) Effects of tropical deforestation on global hydroclimate: A multimodel
952 ensemble analysis. J Clim 22:1124–1141. https://doi.org/10.1175/2008JCLI2157.1
953 Heredia MB, Junquas C, Prieur C, Condom T (2018) New Statistical Methods for Precipitation Bias Correction
954 Applied to WRF Model Simulations in the Antisana Region, Ecuador. J Hydrometeorol 19:2021–2040.
955 https://doi.org/10.1175/JHM-D-18-0032.1
956 Hersbach H, Bell B, Berrisford P, et al (2020) The ERA5 global reanalysis. Q J R Meteorol Soc 146:1999–
957 2049. https://doi.org/10.1002/qj.3803
958 Hohenegger C, Brockhaus P, Schär C (2008) Towards climate simulations at cloud-resolving scales. Meteorol
959 Zeitschrift 17:383–394. https://doi.org/10.1127/0941-2948/2008/0303
960 Hong S-Y, Noh Y, Dudhia J (2006) A New Vertical Diffusion Package with an Explicit Treatment of
961 Entrainment Processes. Mon Weather Rev 134:2318–2341. https://doi.org/10.1175/MWR3199.1
962 Hoorn C, Wesselingh FP, Ter Steege H, et al (2010) Amazonia through time: Andean uplift, climate change,
963 landscape evolution, and biodiversity. Science (80-.).
964 Huffman GJ, Bolvin DT, Nelkin EJ, et al (2007) The TRMM Multisatellite Precipitation Analysis (TMPA):
965 Quasi-Global, Multiyear, Combined-Sensor Precipitation Estimates at Fine Scales. J Hydrometeorol 8:38–
966 55. https://doi.org/10.1175/JHM560.1
967 Ibisch P, Nowicki C, Müller R (2001) El biocorredor Amboró-Madidi – primeros insumos botánicos para un
968 Plan de Conservación. Rev la Soc Boliv Botánica 3:
969 Jiménez PA, Dudhia J (2012) Improving the Representation of Resolved and Unresolved Topographic Effects
970 on Surface Wind in the WRF Model. J Appl Meteorol Climatol 51:300–316.
971 https://doi.org/10.1175/JAMC-D-11-084.1

Junquas C, Takahashi K, Condom T, et al (2018) Understanding the influence of orography on the precipitation diurnal cycle and the associated atmospheric processes in the central Andes. Clim Dyn. https://doi.org/10.1007/s00382-017-3858-8
Kalamandeen M, Gloor E, Mitchard E, et al (2018) Pervasive Rise of Small-scale Deforestation in Amazonia. Sci Rep. https://doi.org/10.1038/s41598-018-19358-2
Kessler M, Kluge J (2008) Diversity and endemism in tropical montane forests - from patterns to processes. Biodivers Ecol Ser 2:
Khanna J, Medvigy D, Fueglistaler S, Walko R (2017) Regional dry-season climate changes due to three decades of Amazonian deforestation. Nat Clim Chang 7:200–204. https://doi.org/10.1038/nclimate3226
Kikuchi K, Wang B (2008) Diurnal Precipitation Regimes in the Global Tropics*. J Clim 21:2680–2696. https://doi.org/10.1175/2007JCLI2051.1
Killeen TJ, Douglas M, Consiglio T, et al (2007) Dry spots and wet spots in the Andean hotspot. In: Journal of Biogeography
Kodama Y (1992) Large-Scale Common Features of Subtropical Precipitation Zones (the Baiu Frontal Zone, the SPCZ, and the SACZ) Part I: Characteristics of Subtropical Frontal Zones. J Meteorol Soc Japan Ser II 70:813–836. https://doi.org/10.2151/jmsj1965.70.4_813
Lawrence D, Vandecar K (2015) Effects of tropical deforestation on climate and agriculture. Nat Clim Chang 5:27–36. https://doi.org/10.1038/nclimate2430
Lean J, Rowntree PR (1997) Understanding the Sensitivity of a GCM Simulation of Amazonian Deforestation to the Specification of Vegetation and Soil Characteristics. J Clim 10:1216–1235. https://doi.org/10.1175/1520-0442(1997)010<1216:UTSOAG>2.0.CO;2
Lee X, Goulden ML, Hollinger DY, et al (2011) Observed increase in local cooling effect of deforestation at higher latitudes. Nature. https://doi.org/10.1038/nature10588
Leite-Filho AT, Costa MH, Fu R (2020) The southern Amazon rainy season: The role of deforestation and its interactions with large-scale mechanisms. Int J Climatol 40:2328–2341. https://doi.org/10.1002/joc.6335
Lenters JD, Cook KH (1997) On the Origin of the Bolivian High and Related Circulation Features of the South American Climate. J Atmos Sci 54:656–678. https://doi.org/10.1175/1520-0469(1997)054<0656:OTOOTB>2.0.CO;2
Li L, Li W, Barros AP (2013) Atmospheric moisture budget and its regulation of the summer precipitation variability over the Southeastern United States. Clim Dyn 41:613–631. https://doi.org/10.1007/s00382-013-1697-9
Li W, Fu R (2004) Transition of the large-scale atmospheric and land surface conditions from the dry to the wet season over Amazonia as diagnosed by the ECMWF re-analysis. J Clim 17:2637–2651. https://doi.org/10.1175/1520-0442(2004)017<2637:TOTLAA>2.0.CO;2
Lin Y-L, Farley RD, Orville HD (1983) Bulk Parameterization of the Snow Field in a Cloud Model. J Clim Appl Meteorol 22:1065–1092. https://doi.org/10.1175/1520-0450(1983)022<1065:BPOTSF>2.0.CO;2
Lindzen RS, Nigam S (1987) On the Role of Sea Surface Temperature Gradients in Forcing Low-Level Winds and Convergence in the Tropics. J Atmos Sci 44:2418–2436. https://doi.org/10.1175/1520-0469(1987)044<2418:OTROSS>2.0.CO;2
Loarie SR, Lobell DB, Asner GP, Field CB (2011) Land-Cover and Surface Water Change Drive Large Albedo Increases in South America*. Earth Interact 15:1–16. https://doi.org/10.1175/2010EI342.1
Machado LAT (2002) Diurnal march of the convection observed during TRMM-WETAMC/LBA. J Geophys Res 107:8064. https://doi.org/10.1029/2001JD000338
Mahowald NM, Ward DS, Doney SC, et al (2017) Are the impacts of land use on warming underestimated in climate policy? Environ Res Lett. https://doi.org/10.1088/1748-9326/aa836d
Malhi Y, Roberts JT, Betts RA, et al (2008) Climate change, deforestation, and the fate of the Amazon. Science (80-) 319:169–172. https://doi.org/10.1126/science.1146961
Marengo JA (2004) Interdecadal variability and trends of rainfall across the Amazon basin. Theor Appl Climatol 78:. https://doi.org/10.1007/s00704-004-0045-8
Marengo JA, Tomasella J, Alves LM, et al (2011) The drought of 2010 in the context of historical droughts in the Amazon region. Geophys Res Lett. https://doi.org/10.1029/2011GL047436
Martinez JA, Dominguez F (2014) Sources of atmospheric moisture for the La Plata River Basin. J Clim. https://doi.org/10.1175/JCLI-D-14-00022.1
Medvigy D, Walko RL, Avissar R (2011) Effects of Deforestation on Spatiotemporal Distributions of Precipitation in South America. J Clim 24:2147–2163. https://doi.org/10.1175/2010JCLI3882.1
Miguez-Macho G, Fan Y (2012) The role of groundwater in the Amazon water cycle: 1. Influence on seasonal streamflow, flooding and wetlands. J Geophys Res Atmos 117:n/a-n/a. https://doi.org/10.1029/2012JD017539
Mlawer EJ, Taubman SJ, Brown PD, et al (1997) Radiative transfer for inhomogeneous atmospheres: RRTM, a validated correlated-k model for the longwave. J Geophys Res Atmos 102:16663–16682.

https://doi.org/10.1029/97JD00237
Molina-Carpio J, Espinoza D, Coritza E, et al (2019) Clima y variabilidad espacial de la ceja de monte y andino húmedo. Ecol Boliv
Moore N, Arima E, Walker R, Ramos da Silva R (2007) Uncertainty and the changing hydroclimatology of the Amazon. Geophys Res Lett 34:L14707. https://doi.org/10.1029/2007GL030157
Moquet JS, Crave A, Viers J, et al (2011) Chemical weathering and atmospheric/soil CO2 uptake in the Andean and Foreland Amazon basins. Chem Geol. https://doi.org/10.1016/j.chemgeo.2011.01.005
Mourre L, Condom T, Junquas C, et al (2016) Spatio-temporal assessment of WRF, TRMM and in situ precipitation data in a tropical mountain environment (Cordillera Blanca, Peru). Hydrol Earth Syst Sci 20:125–141. https://doi.org/10.5194/hess-20-125-2016
Mueller R, Beck SG, Lara R (2002) Potential vegetation based on climate-data in the Bolivian Yungas-forests. Ecol Boliv 37:
Myers N, Mittermeler RA, Mittermeler CG, et al (2000) Biodiversity hotspots for conservation priorities. Nature. https://doi.org/10.1038/35002501
Nepstad D, Soares-Filho BS, Merry F, et al (2009) The end of deforestation in the Brazilian Amazon. Science (80-.).
Nobre CA, Sampaio G, Borma LS, et al (2016) Land-use and climate change risks in the amazon and the need of a novel sustainable development paradigm. Proc Natl Acad Sci U S A 113:10759–10768. https://doi.org/10.1073/pnas.1605516113
Nobre CA, Sellers PJ, Shukla J (1991) Amazonian Deforestation and Regional Climate Change. J Clim. https://doi.org/10.1175/1520-0442(1991)004<0957:adarcc>2.0.co;2
Oguntoyinbo JS (1970) Reflection coefficient of natural vegetation, crops and urban surfaces in Nigeria. Q J R Meteorol Soc 96:430–441. https://doi.org/10.1002/qj.49709640907
Oliver SA, Oliver HR, Wallace JS, Roberts AM (1987) Soil heat flux and temperature variation with vegetation, soil type and climate. Agric For Meteorol 39:257–269. https://doi.org/10.1016/0168-1923(87)90042-6
Patton EG, Sullivan PP, Moeng C-H (2005) The Influence of Idealized Heterogeneity on Wet and Dry Planetary Boundary Layers Coupled to the Land Surface. J Atmos Sci 62:2078–2097. https://doi.org/10.1175/JAS3465.1
Paulson CA (1970) The Mathematical Representation of Wind Speed and Temperature Profiles in the Unstable Atmospheric Surface Layer. J Appl Meteorol 9:857–861. https://doi.org/10.1175/1520-0450(1970)009<0857:TMROWS>2.0.CO;2
Peixoto J., Oort A. (1992) Physics of climate
Perry LB, Seimon A, Kelly GM (2014) Precipitation delivery in the tropical high Andes of southern Peru: new findings and paleoclimatic implications. Int J Climatol 34:197–215. https://doi.org/10.1002/joc.3679
Pielke, R. A. S (1984) Mesoscale Meteorological Modeling. In- ternational Geophysics, Vol. 78, Academic Press, 612 pp.
Pielke RA (2001) Influence of the spatial distribution of vegetation and soils on the prediction of cumulus Convective rainfall. Rev Geophys 39:151–177. https://doi.org/10.1029/1999RG000072
Rabatel A, Francou B, Soruco A, et al (2013) Current state of glaciers in the tropical Andes: a multi-century perspective on glacier evolution and climate change. Cryosph 7:81–102. https://doi.org/10.5194/tc-7-81-2013
Ramírez E, Francou B, Ribstein P, et al (2001) Small glaciers disappearing in the tropical Andes: a case-study in Bolivia: Glaciar Chacaltaya (16 o S). J Glaciol 47:187–194. https://doi.org/10.3189/172756501781832214
Ramos da Silva R, Avissar R (2006) The Hydrometeorology of a Deforested Region of the Amazon Basin. J Hydrometeorol 7:1028–1042. https://doi.org/10.1175/JHM537.1
Rasmussen KL, Choi SL, Zuluaga MD, Houze RA (2013) TRMM precipitation bias in extreme storms in South America. Geophys Res Lett 40:3457–3461. https://doi.org/10.1002/grl.50651
Rodwell MJ, Hoskins BJ (2001) Subtropical Anticyclones and Summer Monsoons. J Clim 14:3192–3211. https://doi.org/10.1175/1520-0442(2001)014<3192:SAASM>2.0.CO;2
Romatschke U, Houze RA (2010) Extreme summer convection in South America. J Clim 23:3761–3791. https://doi.org/10.1175/2010JCLI3465.1
Ruiz-Vásquez M, Arias PA, Martínez JA, Espinoza JC (2020) Effects of Amazon basin deforestation on regional atmospheric circulation and water vapor transport towards tropical South America. Clim Dyn. https://doi.org/10.1007/s00382-020-05223-4
Saad SI, da Rocha HR, Silva Dias MAF, Rosolem R (2010) Can the Deforestation Breeze Change the Rainfall in Amazonia? A Case Study for the BR-163 Highway Region. Earth Interact 14:1–25. https://doi.org/10.1175/2010EI351.1
Saavedra M, Junquas C, Espinoza JC, Silva Y (2020) Impacts of topography and land use changes on the air surface temperature and precipitation over the central Peruvian Andes. Atmos Res 234:104711. https://doi.org/10.1016/j.atmosres.2019.104711

Salati E, Vose PB (1984) Amazon Basin: A System in Equilibrium. Science (80-) 225:129–138. https://doi.org/10.1126/science.225.4658.129
Saleska SR, da Rocha HR, Huete AR, et al (2013) LBA-ECO CD-32 Flux Tower Network Data Compilation, Brazilian Amazon: 1999-2006. https://doi.org///dx.doi.org/10.3334/ORNLDAAC/1174
Scala JR, Garstang M, Tao W, et al (1990) Cloud draft structure and trace gas transport. J Geophys Res 95:17015. https://doi.org/10.1029/JD095iD10p17015
Scheel MLM, Rohrer M, Huggel C, et al (2011) Evaluation of TRMM Multi-satellite Precipitation Analysis (TMPA) performance in the Central Andes region and its dependency on spatial and temporal resolution. Hydrol Earth Syst Sci 15:2649–2663. https://doi.org/10.5194/hess-15-2649-2011
Segura H, Espinoza JC, Junquas C, et al (2020) Recent changes in the precipitation-driving processes over the southern tropical Andes/western Amazon. Clim Dyn 54:2613–2631. https://doi.org/10.1007/s00382-020-05132-6
Shuttleworth WJ, Gash JHC, Lloyd CR, et al (1984) Eddy correlation measurements of energy partition for Amazonian forest. Q J R Meteorol Soc 110:1143–1162. https://doi.org/10.1002/qj.49711046622
Sicart JE (2005) Atmospheric controls of the heat balance of Zongo Glacier (16°S, Bolivia). J Geophys Res 110:D12106. https://doi.org/10.1029/2004JD005732
Sicart JE, Espinoza JC, Quéno L, Medina M (2016) Radiative properties of clouds over a tropical Bolivian glacier: seasonal variations and relationship with regional atmospheric circulation. Int J Climatol 36:3116–3128. https://doi.org/10.1002/joc.4540
Skamarock WC, Klemp JB, Dudhia J, et al (2019) A Description of the Advanced Research WRF Model Version 4 (No. NCAR/TN-556+STR). https://doi.org/10.5065/1dfh-6p97
Snyder PK (2010) The influence of tropical deforestation on the Northern Hemisphere climate by atmospheric teleconnections. Earth Interact. https://doi.org/10.1175/2010EI280.1
Soares-Filho BS, Nepstad DC, Curran LM, et al (2006) Modelling conservation in the Amazon basin. Nature 440:520–523. https://doi.org/10.1038/nature04389
Souza EP, Renno NO, Dias MAFS (2000) Convective circulations induced by surface heterogeneities. J Atmos Sci 57:2915–2922. https://doi.org/10.1175/1520-0469(2000)057<2915:CCIBSH>2.0.CO;2
Spera SA, Winter JM, Chipman JW (2018) Evaluation of Agricultural Land Cover Representations on Regional Climate Model Simulations in the Brazilian Cerrado. J Geophys Res Atmos 123:5163–5176. https://doi.org/10.1029/2017JD027989
Staal A, Tuinenburg OA, Bosmans JHC, et al (2018) Forest-rainfall cascades buffer against drought across the Amazon. Nat Clim Chang 8:539–543. https://doi.org/10.1038/s41558-018-0177-y
Sun X, Barros AP (2015a) Isolating the role of surface evapotranspiration on moist convection along the eastern flanks of the tropical Andes using a quasi-idealized approach. J Atmos Sci 72:243–261. https://doi.org/10.1175/JAS-D-14-0048.1
Sun X, Barros AP (2015b) Impact of Amazonian evapotranspiration on moisture transport and convection along the eastern flanks of the tropical Andes. Q J R Meteorol Soc 141:3325–3343. https://doi.org/10.1002/qj.2615
Swann ALS, Longo M, Knox RG, et al (2015) Future deforestation in the Amazon and consequences for South American climate. Agric For Meteorol 214–215:12–24. https://doi.org/10.1016/j.agrformet.2015.07.006
Trachte K (2018) Atmospheric Moisture Pathways to the Highlands of the Tropical Andes: Analyzing the Effects of Spectral Nudging on Different Driving Fields for Regional Climate Modeling. Atmosphere (Basel) 9:456. https://doi.org/10.3390/atmos9110456
Trachte K, Nauss T, Bendix J (2010) The impact of different terrain configurations on the formation and dynamics of katabatic flows: Idealised case studies. Boundary-Layer Meteorol 134:307–325. https://doi.org/10.1007/s10546-009-9445-8
Van Der Ent RJ, Savenije HHG, Schaefli B, Steele-Dunne SC (2010) Origin and fate of atmospheric moisture over continents. Water Resour Res. https://doi.org/10.1029/2010WR009127
Vauchel P, Santini W, Guyot JL, et al (2017) A reassessment of the suspended sediment load in the Madeira River basin from the Andes of Peru and Bolivia to the Amazon River in Brazil, based on 10 years of data from the HYBAM monitoring programme. J Hydrol. https://doi.org/10.1016/j.jhydrol.2017.07.018
Vera C, Higgins W, Amador J, et al (2006) Toward a Unified View of the American Monsoon Systems. J Clim 19:4977–5000. https://doi.org/10.1175/JCLI3896.1
Vernekar AD, Kirtman BP, Fennessy MJ (2003) Low-Level Jets and Their Effects on the South American Summer Climate as Simulated by the NCEP Eta Model*. J Clim 16:297–311. https://doi.org/10.1175/1520-0442(2003)016<0297:LLJATE>2.0.CO;2
von Randow C, Manzi AO, Kruijt B, et al (2004) Comparative measurements and seasonal variations in energy and carbon exchange over forest and pasture in South West Amazonia. Theor Appl Climatol 78:5–26. https://doi.org/10.1007/s00704-004-0041-z
Wang J, Bars RL, Eltahir EAB (1996) A Stochastic Linear Theory of Mesoscale Circulation Induced by the

Thermal Heterogeneity of the Land Surface. J Atmos Sci 53:3349–3366. https://doi.org/10.1175/1520-0469(1996)053<3349:ASLTOM>2.0.CO;2
Wang J, Bras RL, Eltahir EAB (2000) The Impact of Observed Deforestation on the Mesoscale Distribution of Rainfall and Clouds in Amazonia. J Hydrometeorol 1:267–286. https://doi.org/10.1175/1525-7541(2000)001<0267:TIOODO>2.0.CO;2
Weisman ML, Skamarock WC, Klemp JB (1997) The Resolution Dependence of Explicitly Modeled Convective Systems. Mon Weather Rev 125:527–548. https://doi.org/10.1175/1520-0493(1997)125<0527:TRDOEM>2.0.CO;2
Yang Z, Dominguez F (2019) Investigating land surface effects on the moisture transport over South America with a moisture tagging model. J Clim 32:6627–6644. https://doi.org/10.1175/JCLI-D-18-0700.1
Yoon JH, Zeng N (2010) An Atlantic influence on Amazon rainfall. Clim Dyn. https://doi.org/10.1007/s00382-009-0551-6
Zardi D, Whiteman CD (2013) Diurnal Mountain Wind Systems. pp 35–119
Zemp DC, Schleussner C-F, Barbosa HMJ, Rammig A (2017a) Deforestation effects on Amazon forest resilience. Geophys Res Lett 44:6182–6190. https://doi.org/10.1002/2017GL072955
Zemp DC, Schleussner CF, Barbosa HMJ, et al (2014) On the importance of cascading moisture recycling in South America. Atmos Chem Phys. https://doi.org/10.5194/acp-14-13337-2014
Zemp DC, Schleussner CF, Barbosa HMJ, et al (2017b) Self-amplified Amazon forest loss due to vegetation-atmosphere feedbacks. Nat Commun 8:. https://doi.org/10.1038/ncomms14681
Zeng N, Neelin JD (1999) A Land–Atmosphere Interaction Theory for the Tropical Deforestation Problem. J Clim 12:857–872. https://doi.org/10.1175/1520-0442(1999)012<0857:ALAITF>2.0.CO;2
Zhang H, McGuffie K, Henderson-Sellers A (1996) Impacts of tropical deforestation. Part II: The role of large-scale dynamics. J Clim. https://doi.org/10.1175/1520-0442(1996)009<2498:IOTDPI>2.0.CO;2
Zhou J, Lau K-M (2001) Principal modes of interannual and decadal variability of summer rainfall over South America. Int J Climatol 21:1623–1644. https://doi.org/10.1002/joc.700
Zhuang Y, Fu R, Marengo JA, Wang H (2017) Seasonal variation of shallow-to-deep convection transition and its link to the environmental conditions over the Central Amazon. J Geophys Res Atmos 122:2649–2666. https://doi.org/10.1002/2016JD025993
Zubieta R, Getirana A, Espinoza JC, Lavado W (2015) Impacts of satellite-based precipitation datasets on rainfall–runoff modeling of the Western Amazon basin of Peru and Ecuador. J Hydrol 528:599–612. https://doi.org/10.1016/j.jhydrol.2015.06.064

Figures

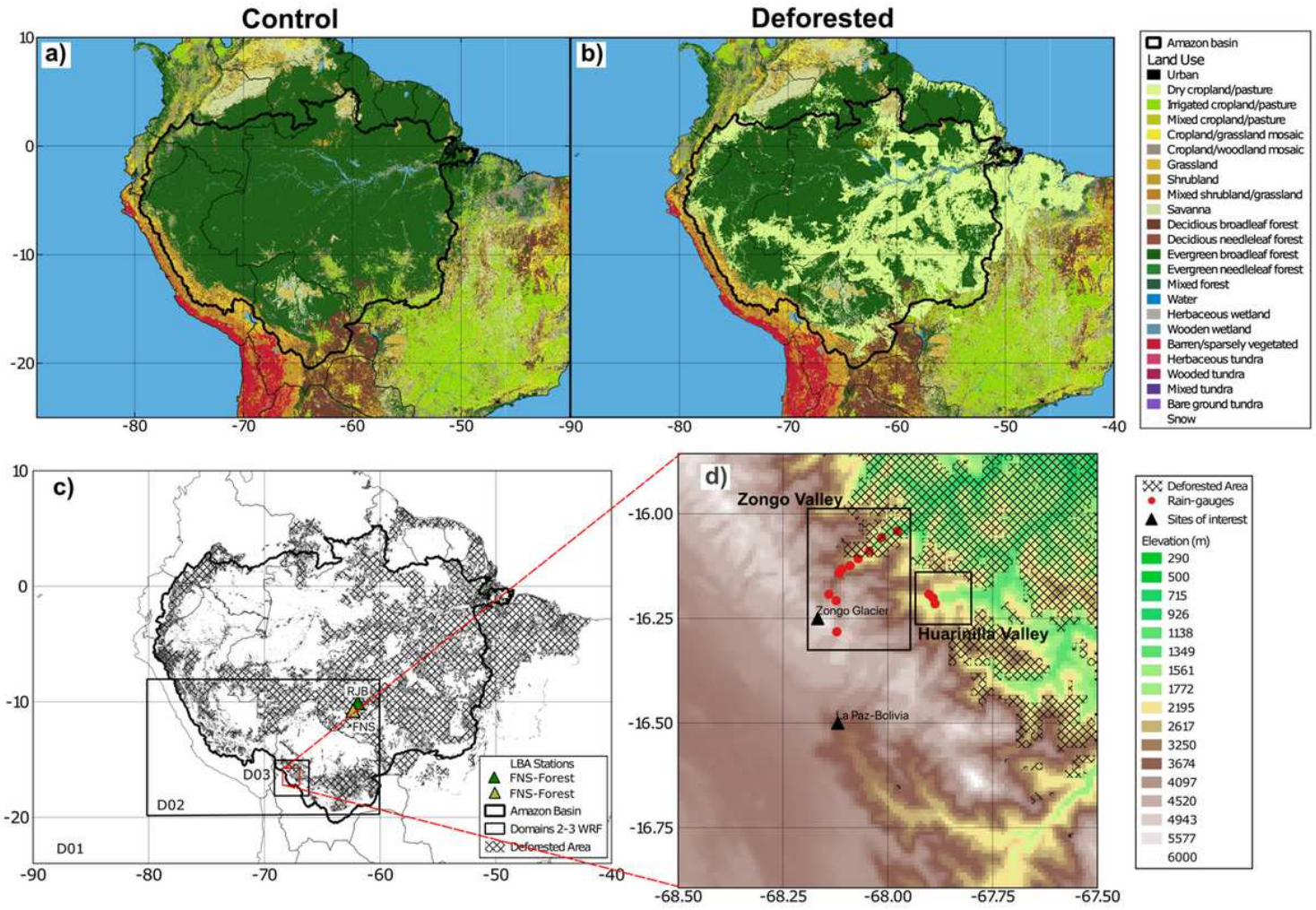

Figure 1

Land-use category distributions for: a) Control and b) Deforested scenarios. c) Deforested area and locations of selected flux towers from the Large-Scale Biosphere-Atmosphere Experiment in the Amazon. Black boxes show WRF domains. Delineated area represents the boundary of the Amazon River basin (black). d) D03 subregion and locations of rain-gauges stations over two Andean mountain valleys Note: The designations employed and the presentation of the material on this map do not imply the expression of any opinion whatsoever on the part of Research Square concerning the legal status of any country, territory, city or area or of its authorities, or concerning the delimitation of its frontiers or boundaries. This map has been provided by the authors.

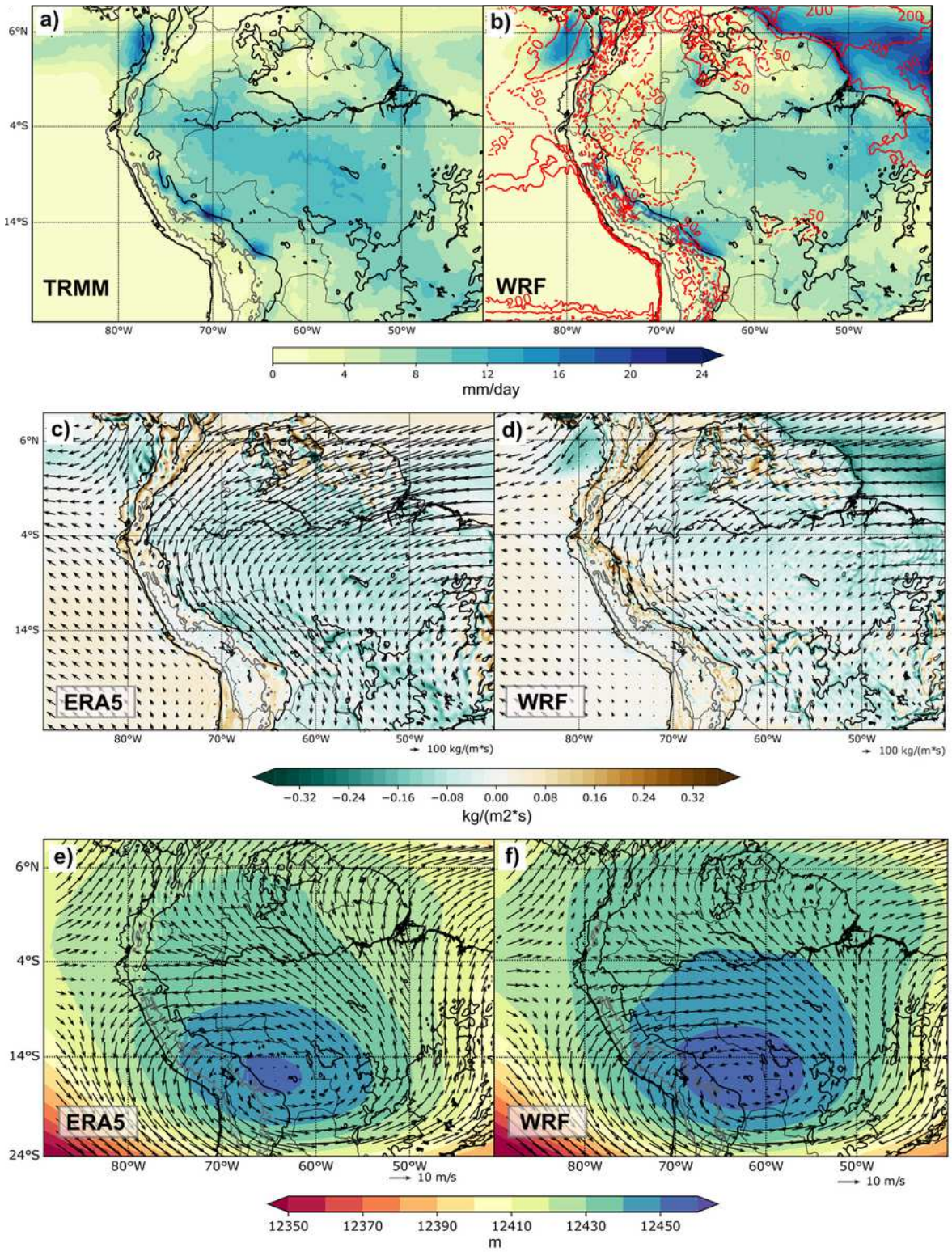

Figure 2

DJF climatological means over the period 2001-2011 for: a) and b) precipitation from TRMM-3B42 (a) and WRF-Control (b) in mm/day. Red lines in b represent rainfall differences respect to TRMM in percentage. c) and d) vertically integrated moisture flux (vectors, kg/m*s) and its divergence (shaded, kg/m2*s) from ERA5 (c) and WRF-Control (d). e) and f) horizontal winds at 200 hPa (vectors, m/s) and geopotential height (shaded, m) from ERA5 (e) and WRF-Control (f). Orography elevation is shown at 500

and 3500 m a.s.l. as black and grey contours, respectively Note: The designations employed and the presentation of the material on this map do not imply the expression of any opinion whatsoever on the part of Research Square concerning the legal status of any country, territory, city or area or of its authorities, or concerning the delimitation of its frontiers or boundaries. This map has been provided by the authors.

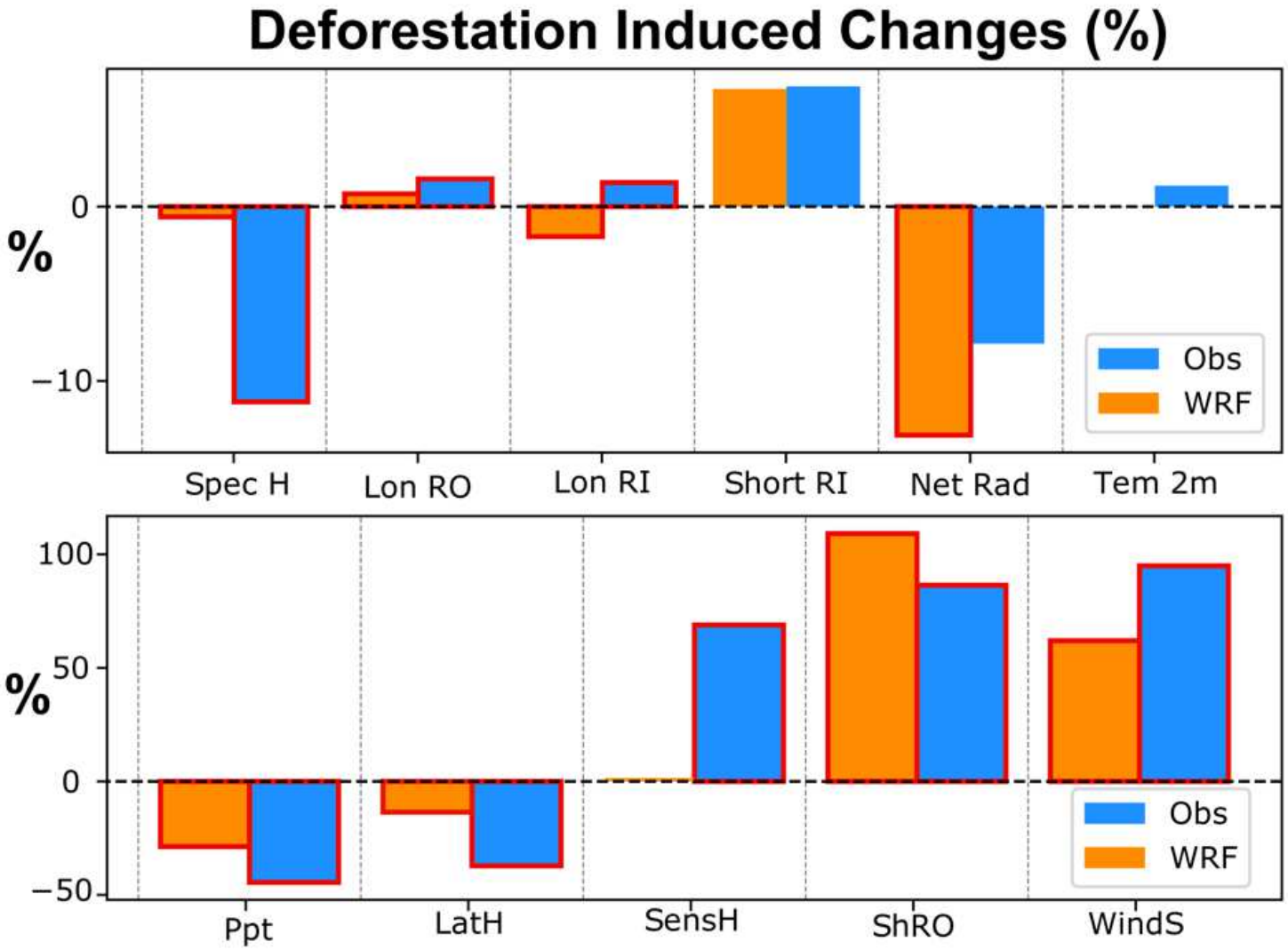

Figure 3

Deforestation induced changes in surface atmospheric variables over LBA stations (blue bars) and WRF-D02 (orange bars) for DJF in the period 2001-2002. Significant differences are delineated in red (t-test, $p<0.05$). Abbreviations are as follows: Spec H - specific humidity at 2 m, Lon RO – longwave outgoing radiation, Lon RI – longwave incoming radiation, Short RO – shortwave outgoing radiation, Short RI – shortwave incoming radiation, Net-Rad – net radiation, Tem2 2m – air temperature at 2 m, LatH – latent heat flux, SensH – sensible heat flux, Ppt – precipitation, WindS – wind speed at 10 m

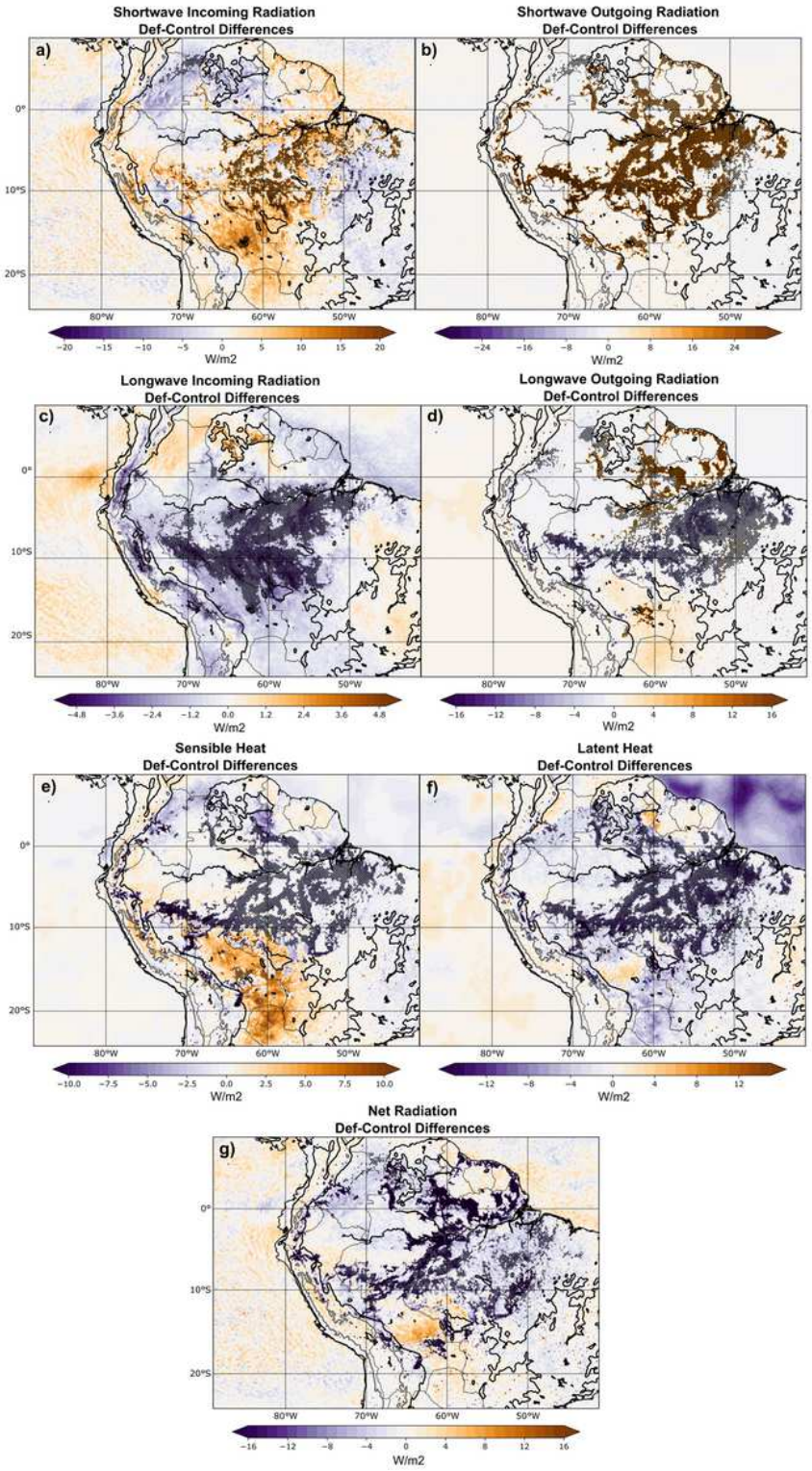

Figure 4

"Please see the Manuscript PDF file for the complete figure caption." Note: The designations employed and the presentation of the material on this map do not imply the expression of any opinion whatsoever on the part of Research Square concerning the legal status of any country, territory, city or area or of its authorities, or concerning the delimitation of its frontiers or boundaries. This map has been provided by the authors.

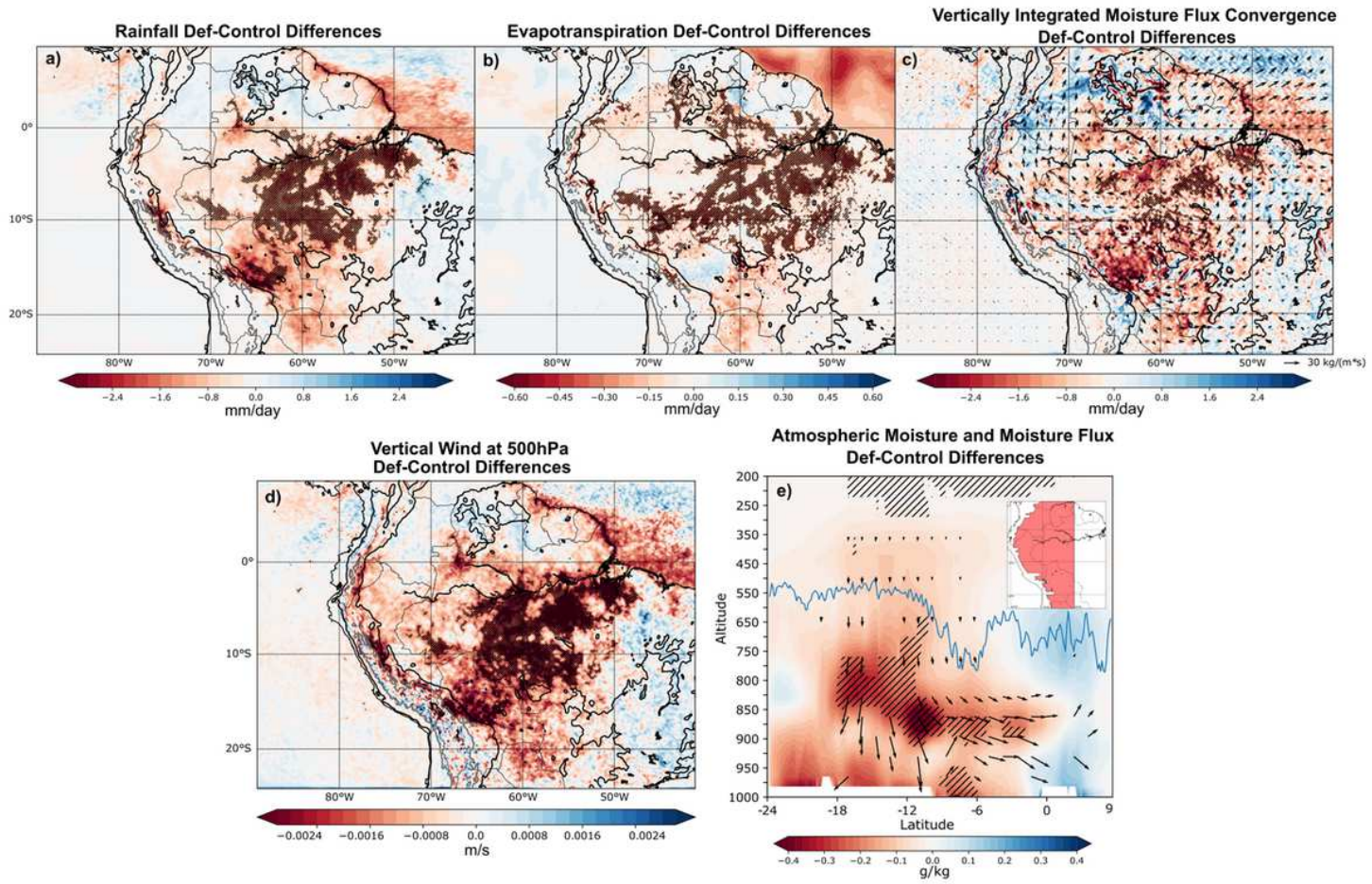

Figure 5

"Please see the Manuscript PDF file for the complete figure caption." Note: The designations employed and the presentation of the material on this map do not imply the expression of any opinion whatsoever on the part of Research Square concerning the legal status of any country, territory, city or area or of its authorities, or concerning the delimitation of its frontiers or boundaries. This map has been provided by the authors.

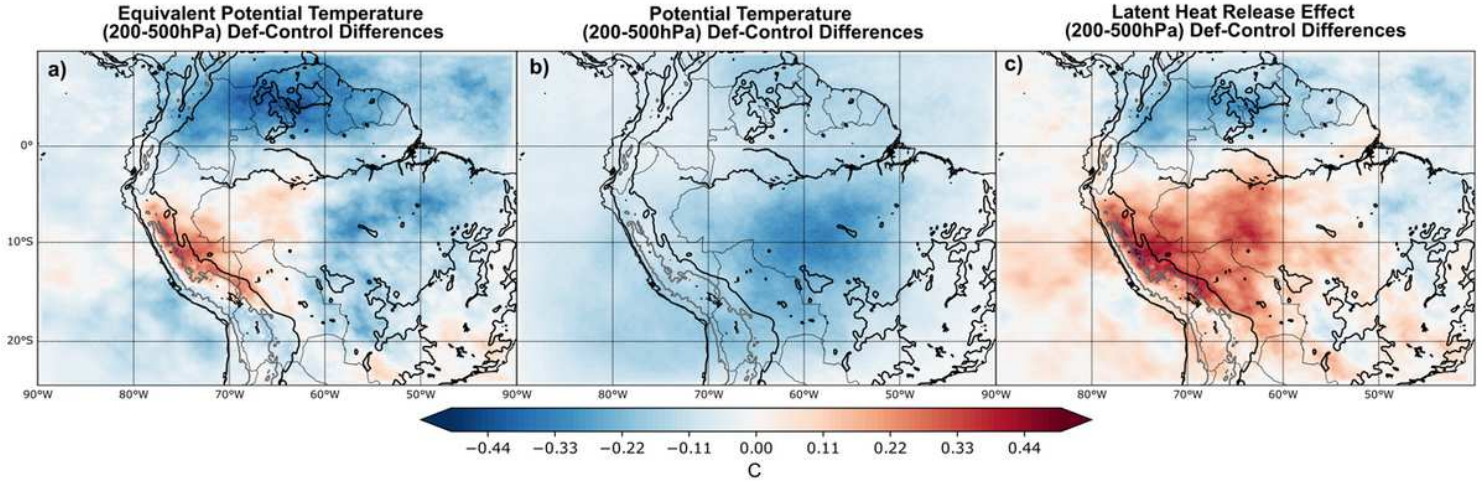

Figure 6

"Please see the Manuscript PDF file for the complete figure caption." Note: The designations employed and the presentation of the material on this map do not imply the expression of any opinion whatsoever on the part of Research Square concerning the legal status of any country, territory, city or area or of its authorities, or concerning the delimitation of its frontiers or boundaries. This map has been provided by the authors.

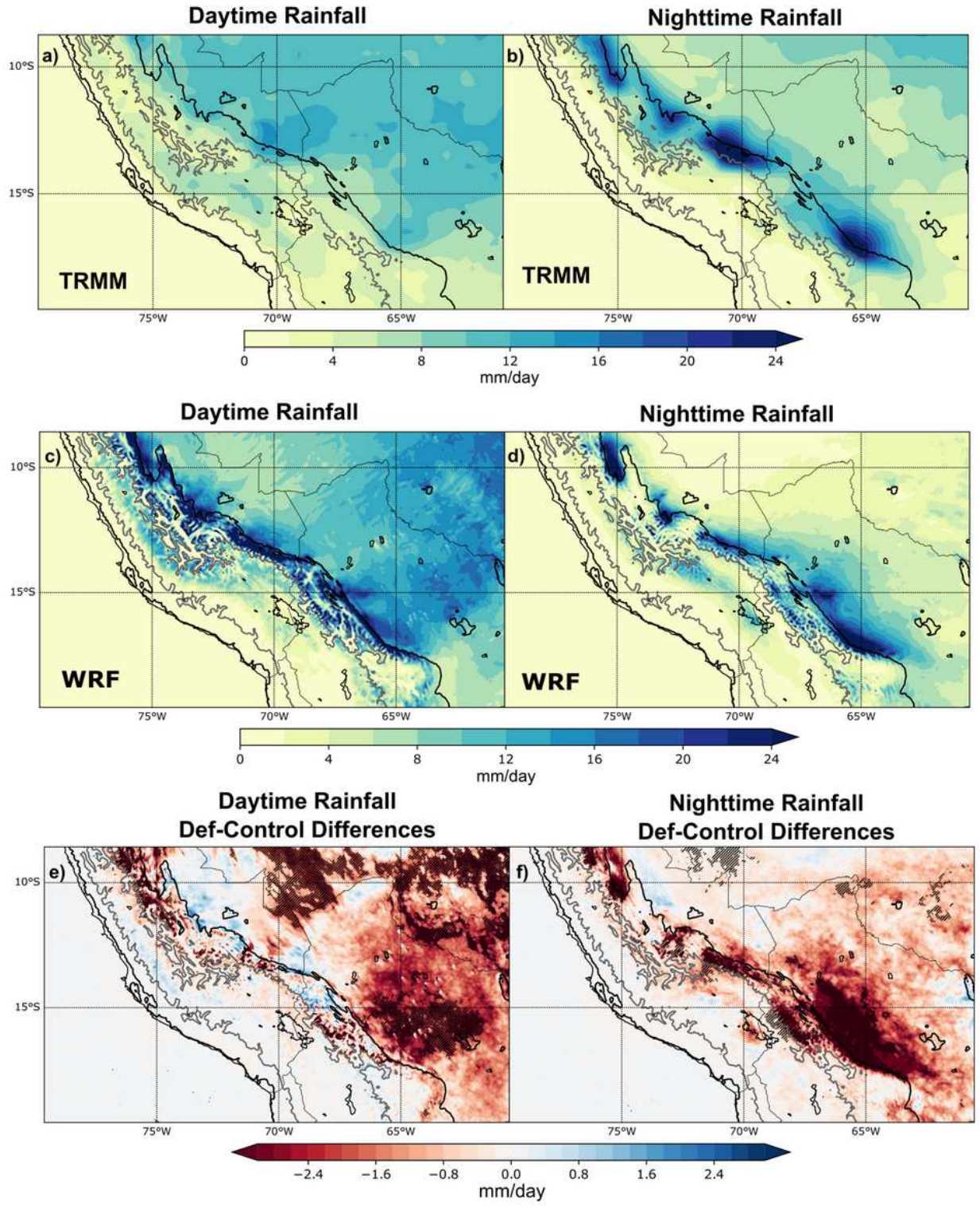

Figure 7

DJF climatological means (2001-2011) for daytime and nighttime precipitation from: a-b) TRMM-3B42. c-510 d) WRF-D02. e-f) WRF-D02 Deforested-Control differences. All figures are in mm/day. Significant changes (t-511 test, p<0.05) are marked with black slashes. Orography elevation is shown at 500 and 3500 m a.s.l. as black and 512 grey contours, respectively Note: The designations employed and the presentation of the material on this map do not imply the expression of any opinion whatsoever on the part of Research Square concerning the legal status of any country, territory, city or area or of its authorities, or concerning the delimitation of its frontiers or boundaries. This map has been provided by the authors.

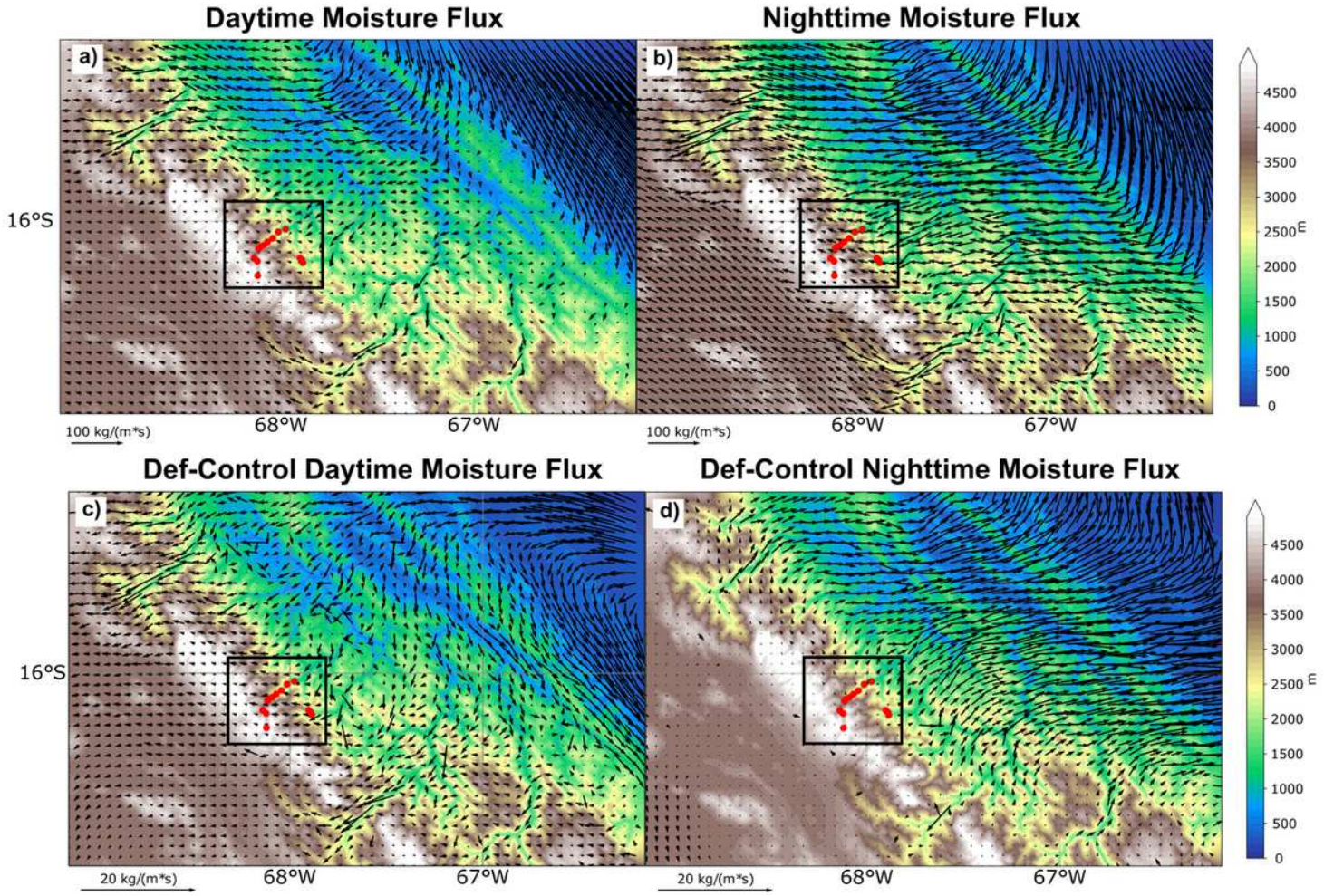

Figure 8

DJF climatological means (2001-2011) for daytime and nighttime vertically-integrated moisture flux from 568 WRF-D03r: a-b) Control and c-d) Deforested minus Control differences. Terrain elevation (shaded) in m and rain-569 gauge stations (red dots). The black square shows the area where the Andean valleys of Huarinilla and Zongo are 570 located Note: The designations employed and the presentation of the material on this map do not imply the expression of any opinion whatsoever on the part of Research Square concerning the legal status of any country, territory, city or area or of its authorities, or concerning the delimitation of its frontiers or boundaries. This map has been provided by the authors.

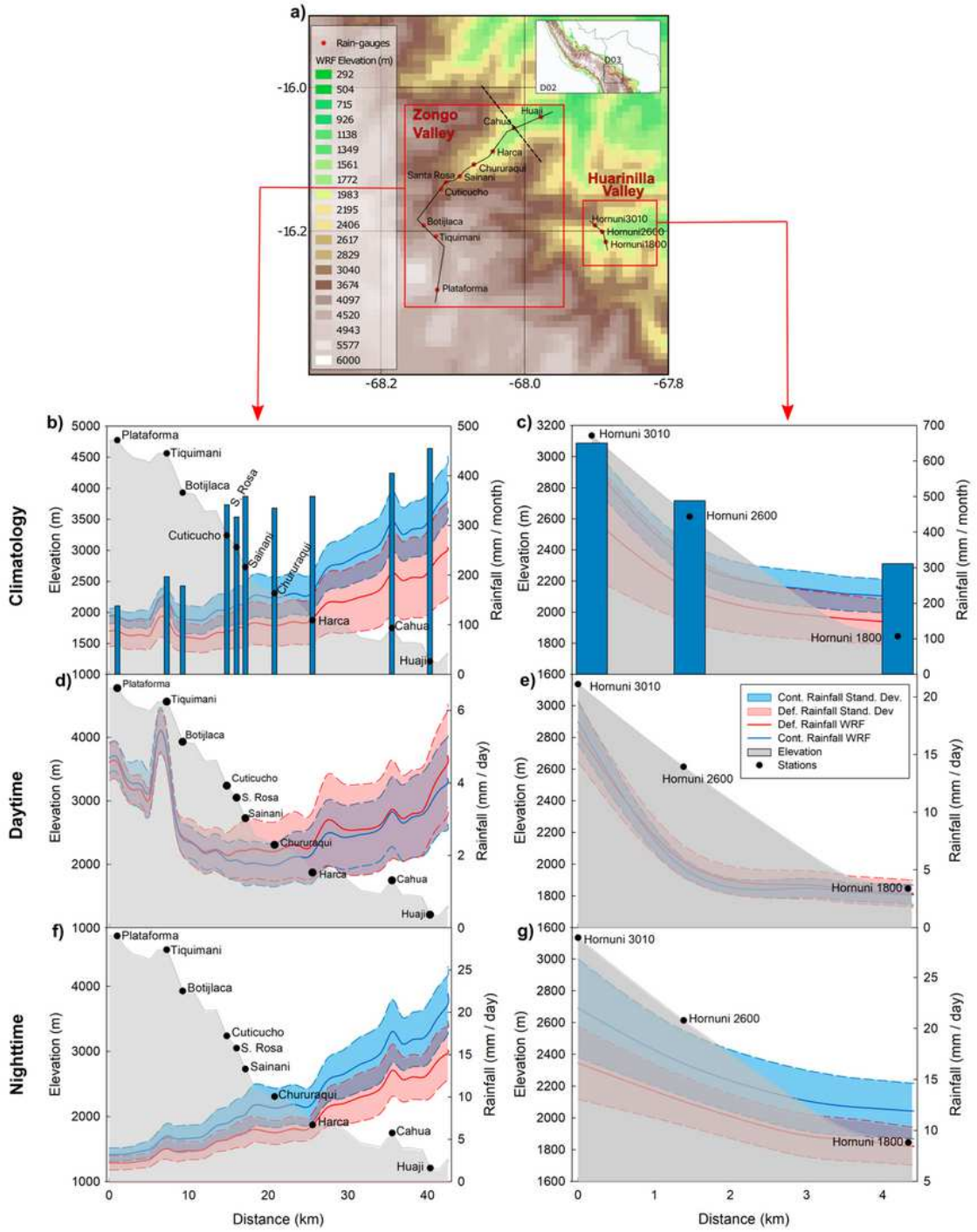

Figure 9

a) Map of the subregion inside D03 with terrain elevation (shaded) in m and rain-gauge stations (red dots). 662 Two selected cross-sections are indicated in black solid lines. A perpendicular cross-section in Zongo Valley 663 shown in Figure 10 is indicated as a dashed black line. b-c) Cross-sections for b) Zongo Valley and c) Huarinilla 664 Valley. Topographical profiles are displayed as a gray line (in m). Observed rain-gauge rainfall is presented as 665 blue bars. WRF-D03 Control and Deforested rainfall

climatological means are shown as blue and red lines and 666 are labeled as Cont. and Def., respectively. Rainfall is in mm/month. d-g) Same as Fig. 9b-c but for daytime and 667 nighttime conditions. Rainfall is in mm/day. The x axis represents the horizontal distance in km along the cross-668 sections. Blue and red envelopes represent model standard deviation for each scenario. Black dots represent rain-669 gauge stations Note: The designations employed and the presentation of the material on this map do not imply the expression of any opinion whatsoever on the part of Research Square concerning the legal status of any country, territory, city or area or of its authorities, or concerning the delimitation of its frontiers or boundaries. This map has been provided by the authors.

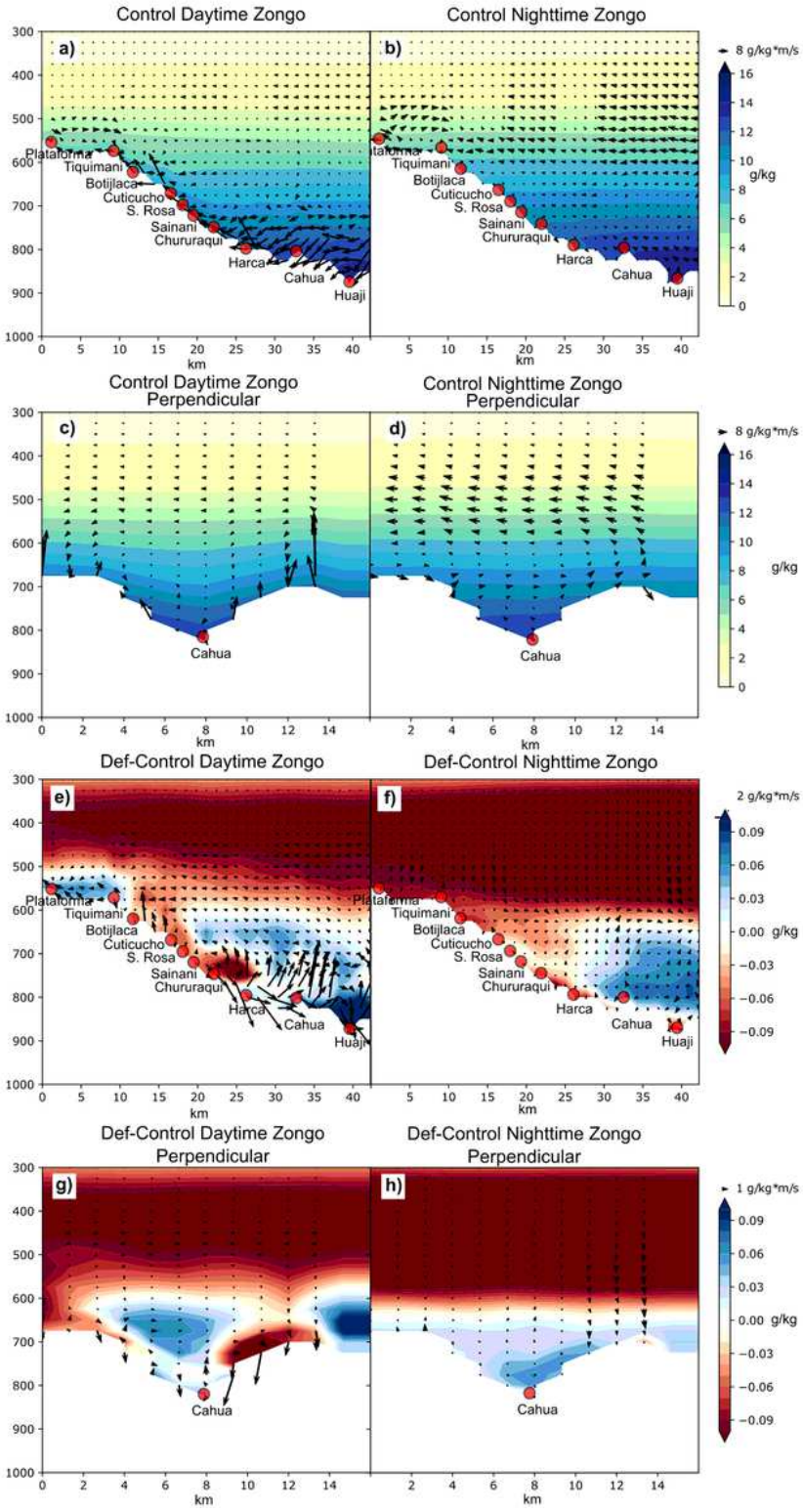

Figure 10

Vertical cross-section for daytime and nighttime DJF climatological means (2001-2011) in atmospheric 687 moisture (shaded, g/kg) and moisture flux (vectors, g/kg*m/s) for the Zongo Valley in two opposite directions: 688 28 parallel to the transect (see black solid line in Fig. 9a) and perpendicular to the transect (see black dashed line in 689 Fig. 9a). Daytime (a) and nighttime (b) WRF-Control conditions for the transect parallel to the Zongo Valley. 690 Daytime (c) and nighttime (d) WRF-Control conditions for the

transect perpendicular to the Zongo Valley. 691 Daytime (e) and nighttime (f) Deforested minus Control differences in the transect parallel to the Zongo Valley. 692 Daytime (g) and nighttime (h) Deforested minus Control differences in the transect perpendicular to the Zongo 693 Valley. Red dots represent rain-gauge stations. Vertical component of the moisture flux is exaggerated by a factor 694 of ten Note: The designations employed and the presentation of the material on this map do not imply the expression of any opinion whatsoever on the part of Research Square concerning the legal status of any country, territory, city or area or of its authorities, or concerning the delimitation of its frontiers or boundaries. This map has been provided by the authors.

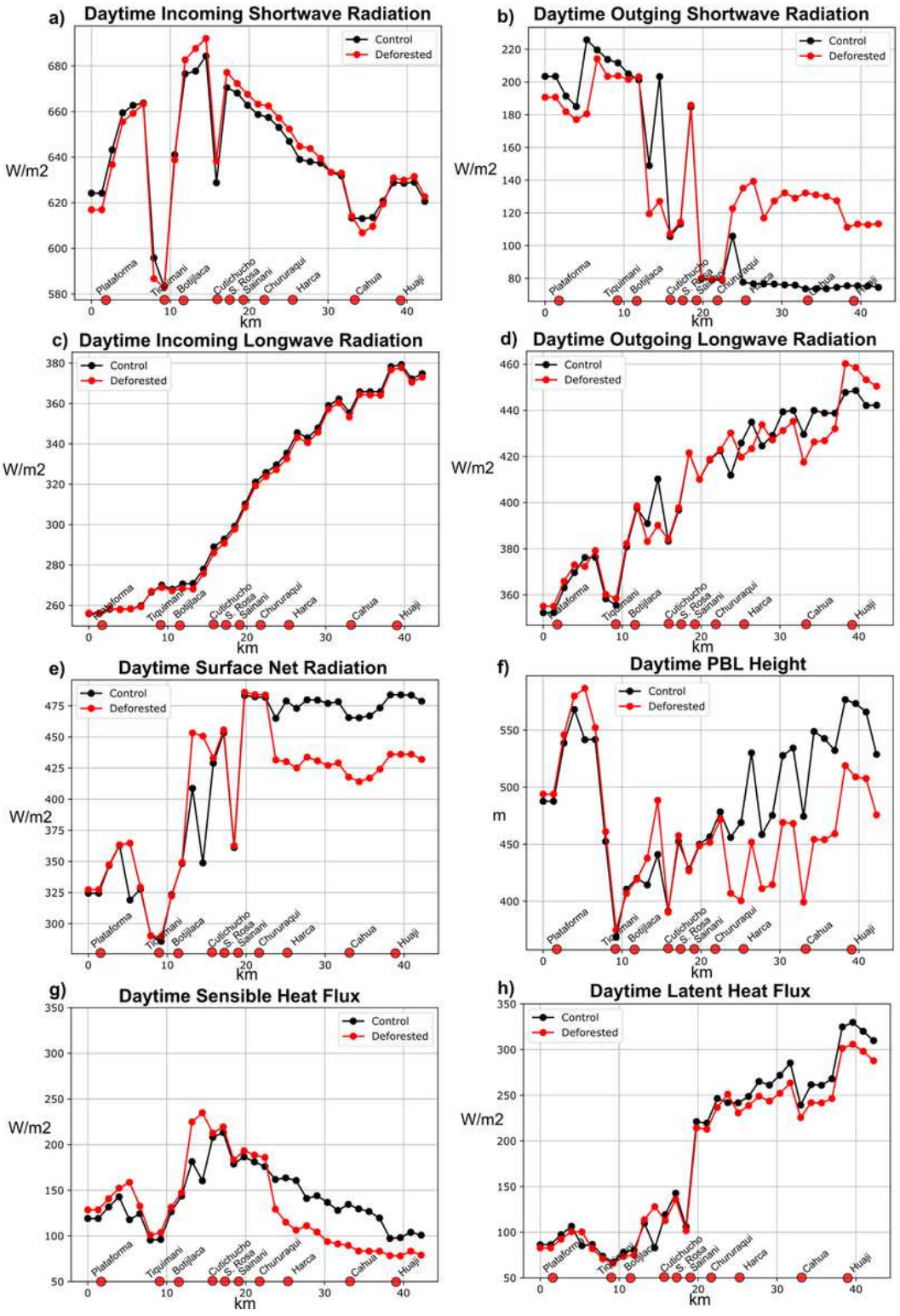

Figure 11

WRF-D03 daytime mean variation along the Zongo Valley transect in Control and Deforested scenarios 698 (black and red lines, respectively) for: a) Shortwave incoming radiation. b) Shortwave outgoing radiation. c) 699 30 Longwave incoming radiation. d) Longwave outgoing radiation. e) Surface net radiation. f) Planetary boundary 700 layer (PBL) height. g) Sensible heat flux. h) Latent heat flux. Red dots represent rain-gauge stations

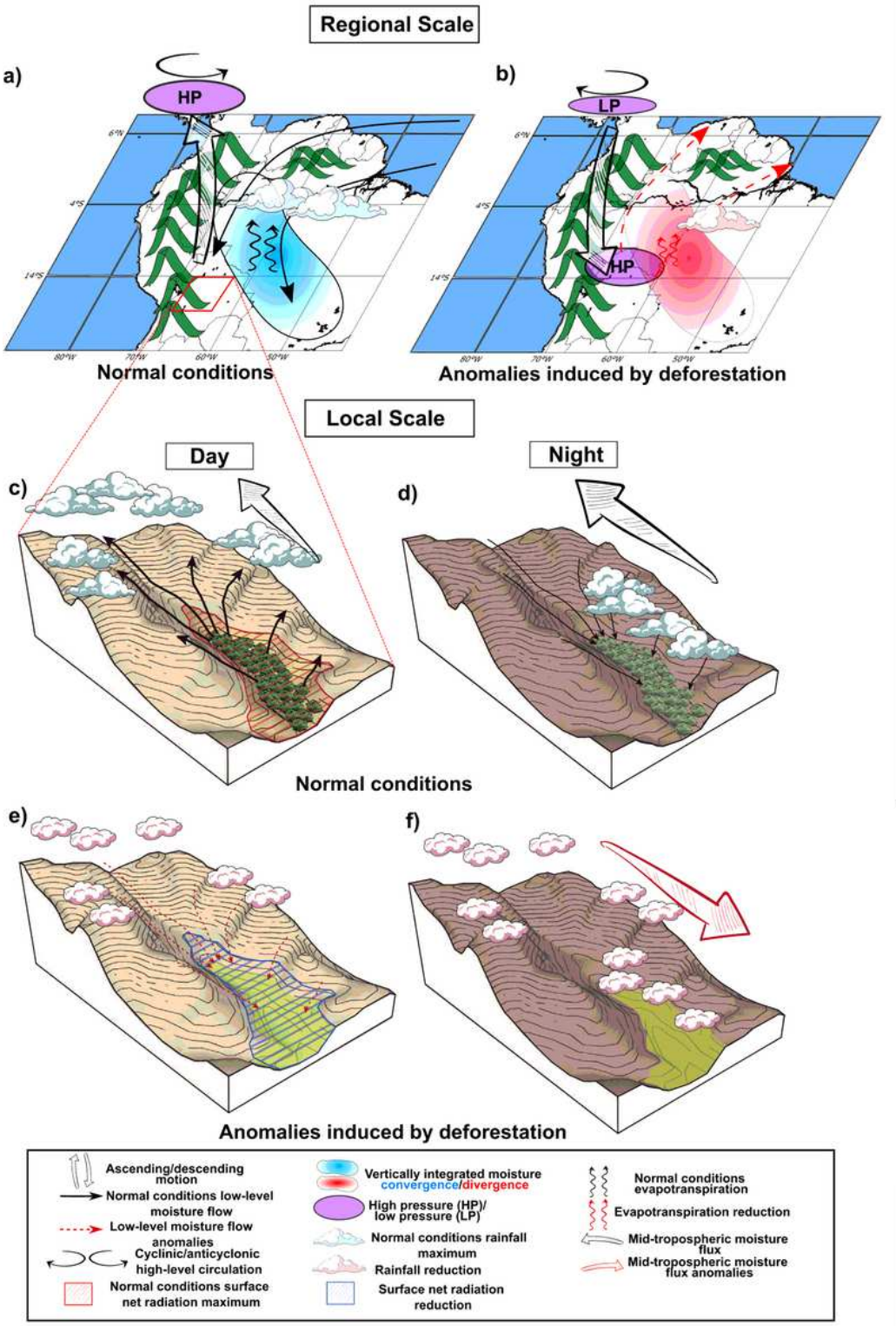

Figure 12

Schematic representation of DJF climatological atmospheric conditions at regional (a-b) and local scales 718 (c-f) for normal conditions (a-c-d) and deforestation induced anomalies (b-e-f) in WRF simulations. The red 719 square in a indicates the approximated location of the Zongo Valley sketched in c-f. Black solid (red dashed) thin 720 arrows represent surface moisture transport under normal conditions (deforestation anomalies). Black (red) thick 721 32 arrows represent mid-tropospheric moisture flux under

normal conditions (deforestation anomalies). Vertical 722 thick arrows represent ascending and descending motions. Black (red) curved arrows represent evapotranspiration 723 under normal conditions (deforestation anomalies). Blue and red shaded areas indicate vertically integrated 724 moisture convergence and divergence, respectively. Purple areas indicate pressure changes. Blue and red clouds 725 indicate rainfall maximum and rainfall reductions under normal and deforested conditions, respectively. Red 726 (blue) hatched area in c (e) indicates surface net radiation maximum (reduction) under normal (deforestation) 727 conditions